



**HAL**  
open science

# A new chimeric triple reporter fusion protein as a tool for in vitro and in vivo multimodal imaging to monitor the development of African trypanosomes and *Leishmania* parasites

Estefania Calvo-Alvarez, Christelle Cren-Travaillé, Aline Crouzols, Brice Rotureau

## ► To cite this version:

Estefania Calvo-Alvarez, Christelle Cren-Travaillé, Aline Crouzols, Brice Rotureau. A new chimeric triple reporter fusion protein as a tool for in vitro and in vivo multimodal imaging to monitor the development of African trypanosomes and *Leishmania* parasites. *Infection, Genetics and Evolution*, 2018, 10.1016/j.meegid.2018.01.011 . pasteur-01849818

**HAL Id: pasteur-01849818**

**<https://pasteur.hal.science/pasteur-01849818>**

Submitted on 3 Aug 2018

**HAL** is a multi-disciplinary open access archive for the deposit and dissemination of scientific research documents, whether they are published or not. The documents may come from teaching and research institutions in France or abroad, or from public or private research centers.

L'archive ouverte pluridisciplinaire **HAL**, est destinée au dépôt et à la diffusion de documents scientifiques de niveau recherche, publiés ou non, émanant des établissements d'enseignement et de recherche français ou étrangers, des laboratoires publics ou privés.

1 **A new chimeric triple reporter fusion protein as a tool for *in vitro***  
2 **and *in vivo* multimodal imaging to monitor the development of**  
3 **African trypanosomes and *Leishmania* parasites.**

4  
5 Estefania Calvo Alvarez\*, Christelle Cren-Travaillé, Aline Crouzols and Brice Rotureau

6  
7 Trypanosome Transmission Group, Trypanosome Cell Biology Unit, Institut Pasteur and  
8 INSERM U1201, Paris, France

9 \* Corresponding author: Estefania Calvo Alvarez, estefania.calvo-alvarez@pasteur.fr

10  
11 **Key words:** *Trypanosoma*, *Leishmania*, bioluminescence, fluorescence, intravital imaging,  
12 fusion protein, reporter.

13  
14 **Short title:** A triple reporter for multimodal imaging of trypanosomatids

15  
16 Number of figures: 8 (+3)

17 **Highlights**

- 18 • New triple reporter combining a red luciferase and a tdTomato fused by a Ty1-tag  
19 • Tested in two different stages of both *T. brucei* and *L. major* parasites  
20 • Tested *in vitro* and *in vivo* in tsetse flies and murine models  
21 • Useful for multimodal imaging at different scales, including intravital monitoring  
22

23 **Abstract**

24 Trypanosomiasis and leishmaniasis, caused by a group of related protist parasites, are  
25 Neglected Tropical Diseases currently threatening more than 500 million people worldwide.  
26 Reporter proteins have revolutionised the research on infectious diseases and have opened  
27 up new advances in the understanding of trypanosomatid-borne diseases in terms of both  
28 biology, pathogenesis and drug development. Here, we describe the generation and some  
29 applications of a new chimeric triple reporter fusion protein combining the red-shifted firefly  
30 luciferase PpyREH9 and the tdTomato red fluorescent protein, fused by the TY1 tag.  
31 Expressed in both *Trypanosoma brucei brucei* and *Leishmania major* transgenic parasites,  
32 this construct was successfully assessed on different state-of-the-art imaging technologies,  
33 at different scales ranging from whole organism to cellular level, both *in vitro* and *in vivo* in  
34 murine models. For *T. b. brucei*, the usefulness of this triple marker to monitor the entire  
35 parasite cycle in both tsetse flies and mice was further demonstrated. This stable reporter  
36 allows to qualitatively and quantitatively scrutinize in real-time several crucial aspects of the  
37 parasite's development, including the development of African trypanosomes in the dermis of  
38 the mammalian host. We briefly discuss developments in bio-imaging technologies and  
39 highlight how we could improve our understanding of parasitism by combining the genetic  
40 engineering of parasites to the one of the hosting organisms in which they complete their  
41 developmental program.

## 42           1. Introduction

43 Vector-borne diseases affect about half of the World's population and are endemic in more  
44 than 100 countries. Among these vector-borne diseases, trypanosomiasis and  
45 leishmaniasis are considered as important Neglected Tropical Diseases (NTDs) that  
46 especially impact public health, accounting for ~24 million persons infected worldwide among  
47 over 500 million people at risk. These diseases are (i) Human African Trypanosomiasis  
48 (HAT) or sleeping sickness that is caused by the African trypanosomes *Trypanosoma brucei*  
49 (Buscher et al., 2017; Franco et al., 2017), (ii) Chagas disease or American Trypanosomiasis  
50 that is due to the American trypanosome *Trypanosoma cruzi* (Perez-Molina and Molina,  
51 2017; Stanaway and Roth, 2015), and (iii) leishmaniasis, a group of visceral and cutaneous  
52 diseases caused by a wide range of *Leishmania spp.* (Alvar et al., 2012; Matlashewski et al.,  
53 2014; Reithinger et al., 2007). In addition, some other trypanosome species (mainly *T.*  
54 *evansi*, *T. equiperdum*, *T. congolense* and *T. vivax*) cause similar diseases in domestic  
55 animals and are responsible for important economic losses in developing countries  
56 (Rotureau and Van Den Abbeele, 2013). There is no vaccine against these parasites, most  
57 of the few currently available medications are not easily administrable and frequently present  
58 severe side effects, and drug resistance is dramatically increasing. However, in addition to  
59 mass screening and treatment programs, strategies for reservoir and / or vector control have  
60 proven their efficiency in certain endemic areas (Aksoy et al., 2017; Dias, 2015; Gonzalez et  
61 al., 2015).

62 *In vivo* intravital imaging methods have tremendously been improved over the last decades,  
63 and now represent powerful tools for the understanding of a large panel of dynamic biological  
64 processes, especially in the field of infectious diseases (Coombes and Robey, 2010).  
65 Beyond their obvious contribution to the ethical improvement of the experimental design of  
66 research studies on living animals, especially in terms of reduction and refinement, these  
67 approaches also offer a powerful and almost unbiased mean to monitor and compare the  
68 variable kinetics of infection among individuals. In the context of diagnostic tool and drug  
69 development, as well as in order to study the complex developmental cycles of  
70 trypanosomatid parasites, genetically engineered parasites have been developed to express  
71 a large panel of molecular reporters including fluorescent and bioluminescent probes both in  
72 *T. cruzi* (Lewis et al., 2015) and *T. brucei* (Burrell-Saward et al., 2015; Coles et al., 2017;  
73 MacLean et al., 2013; McLatchie et al., 2013; Van Reet et al., 2014), and especially in  
74 *Leishmania spp.* (Beattie and Kaye, 2011; Calvo-Alvarez et al., 2015a; Carneiro et al., 2017;  
75 Forestier, 2013; Lang et al., 2009; Taheri et al., 2015).

76 The choice of a given reporter is conditioned by that of a specific readout methodology that  
77 usually focuses on parasite detection at a single scale, *i.e.* at the cellular level in multi-well  
78 plates for drug screening, at the tissue level in *ex vivo* organ explants or models, at the entire

79 organism level to study the kinetics of the infection in lab animal models. However, only few  
80 attempts to combine these modes of detection and / or imaging have been proposed,  
81 especially in trypanosomatid research (Taheri et al., 2015). From the literature, dual reporter  
82 fusion proteins have been designed for the purpose of combining bioluminescence and  
83 fluorescence-based approaches: firefly luciferase Luc and EGFP (Patel et al., 2010; Taheri et  
84 al., 2015), firefly luciferase Luc2 and EGFP (Liu et al., 2010), firefly luciferase Luc2 and  
85 tdTomato (Liu et al., 2010), firefly luciferase Luc2 and TurboFP635 (Mezzanotte et al., 2014),  
86 mVenus and *Renilla* luciferase RLuc8, mTurquoise2 and RLuc8, mKusabiraOrange2 and  
87 RLuc8 (Takai et al., 2015). All these constructs encode for at least one marker emitting in the  
88 green. This is not optimal for intravital imaging due to the high absorption of the light at these  
89 wavelengths by the melanin and haemoglobin proteins present in tissues. To bypass this  
90 technical bias, McLatchie and colleagues have first reported a system that allows the  
91 detection of fewer than 100 bioluminescent *T. brucei* parasites in a murine model by the use  
92 of the codon-optimised red-shifted *Photinus pyralis* luciferase (PpyRE9H) (McLatchie et al.,  
93 2013). They were able to monitor in real time the parasite dissemination and to detect brain  
94 infections with a level of sensitivity *in vivo* that was significantly greater than achievable with  
95 a yellow firefly luciferase reporter (McLatchie et al., 2013). Almost at the same time, Van  
96 Reet *et al.* have compared the usefulness of three different red-shifted luciferases, and  
97 characterized their *in vitro* activity and growth profile, as well as their potential for *in vivo*  
98 murine infection follow-up in a set of diverse *T. brucei* strains (Van Reet et al., 2014). Burrell-  
99 Saward and co-workers also used the red bioluminescent *T. b. brucei* strain generated by  
100 McLatchie *et al.* to evaluate the efficacy of novel drugs *in vivo* against late-stage HAT and  
101 were able to detect drug relapse earlier than traditional methods (Burrell-Saward et al.,  
102 2015). In order to go a step further, we have selected and combined two reporters producing  
103 light in the red wavelengths (tdTomato at 581nm and red-shifted firefly luciferase PpyREH9  
104 at 617nm) with a reduced absorption in tissues, therefore resulting in an enhanced sensitivity  
105 of the monitoring.

106 Common protocols, such as for electron microscopy, histology or protein biochemistry, can  
107 require deleterious heat and / or chemical treatments of the samples that frequently result in  
108 a denaturation of these recombinant proteins preventing further fluorescent emission,  
109 enzymatic activities as well as immuno-detection. To circumvent these obstacles, the Ty1  
110 epitope has become a popular choice in trypanosomes, but also in other parasites such as  
111 *Leishmania* and *Toxoplasma* (Bastin et al., 1996). The Ty-tag is a 10-amino-acid sequence  
112 from the immunologically well-characterized major structural protein of the Ty1 virus-like  
113 particle of *Saccharomyces cerevisiae* (Brookman et al., 1995). The epitope is recognized by  
114 two different monoclonal antibodies, BB2 (IgG1) and TYG5 (IgA), that were tested in a  
115 variety of immunological conditions and that do not cross-react with trypanosome proteins.

116 Although a number of commercial antibodies from various companies are available against  
117 either firefly luciferase or tdTomato, the Ty1-tag has been used extensively in  
118 Trypanosomatids and it has already proved its usefulness in multiple contexts (Huet et al.,  
119 2014; Julkowska and Bastin, 2009; Ooi et al., 2015). Therefore, between the two red-emitting  
120 probes, we have inserted a small Ty1-tag (Bastin et al., 1996) that can be detected in most of  
121 conditions, in order to obtain a stable cytosolic triple marker fusion protein  
122 (PpyRE9H/TY1/tdTomato) that can be used to study the same sample by multi-modal  
123 detection and imaging approaches.

124 Here, we describe the generation of this new chimeric triple reporter fusion protein. This  
125 construct was successfully assessed on state-of-the-art imaging technologies both *in vitro*  
126 and *in vivo* by using *Trypanosoma brucei* and *Leishmania major* transgenic parasites. This  
127 approach allowed us to scrutinize the development of both parasites within the mammalian  
128 host, as well as the journey of African trypanosomes in the tsetse fly digestive tract.

129 **2. Material and methods**

130 **2.1 Leishmania major and Trypanosoma brucei brucei strains and culture**

131 The AnTat 1.1E pleomorphic clone of *Trypanosoma brucei brucei* was derived from a strain  
132 originally isolated from a bushbuck in Uganda in 1966 (Le Ray et al., 1977). Procyclic forms  
133 (PCF) were grown at 27°C in SDM-79 medium (Brun and Schonenberger, 1979)  
134 supplemented with 10% (v/v) heat-inactivated foetal calf serum (FCS) and 8 mM glycerol  
135 (SDMG). Bloodstream forms (BSF) of the same strain were cultivated in complete HMI-11  
136 medium (Kooy et al., 1989) at 37°C in 5% CO<sub>2</sub>. For *in vitro* slender to stumpy BSF  
137 differentiation, we used 8-pCPT-2'-O-Me-5'-AMP, a nucleotide analog of 5'-AMP from  
138 BIOLOG Life Science Institute (Germany). Briefly, 2x10<sup>6</sup> pleomorphic AnTat 1.1E slender  
139 forms were incubated with 8-pCPT-2'-O-Me-5'-AMP (5 µM) for 48 h (Barquilla et al., 2012).  
140 Freshly differentiated stumpy forms were then centrifuged and resuspended in SDMG  
141 medium with 10 mM glutathione for tsetse fly infection.

142 *Leishmania major* strain Friedlin V1 (MHOM/JL/80/Friedlin) (Kapler et al., 1990), was  
143 cultured at 26°C in M199 supplemented with 25 mM HEPES pH 7.2, 0.1 mM adenine,  
144 0.0005% (w/v) hemin, 2 µg/ml bioppterin, 0.0001% (w/v) biotin, 10% (v/v) FCS and antibiotic  
145 cocktail (50 U/ml penicillin, 50 µg/ml streptomycin).

146 **2.2 Construction of the chimeric fusion DNA sequences**

147 A 3.1 Kb sequence coding for the chimeric multiplex reporter protein  
148 PpyRE9H/TY1/tdTomato was genetically engineered. The resulting cytoplasmic reporter is  
149 composed of three distinct markers: the red-shifted luciferase (PpyRE9H) is fused to the  
150 tdTomato red fluorescent protein by a Ty1 tag.

151 To generate RED *T. brucei* parasites, the 1.68 Kb optimised version of the North American  
152 firefly *Photinus pyralis* luciferase (Branchini et al., 2005) was fused with a 30-bp sequence  
153 known as Ty1-tag (Bastin et al., 1996) and cloned into the pTSARib plasmid (Xong et al.,  
154 1998) by using *Xho*I and *Hind*III restriction enzymes to obtain the pTSARib-PpyRE9H-TY1  
155 plasmid. Finally, the 1.4 Kb coding region of the tdTomato fluorescent protein was inserted  
156 downstream using *Hind*III and *Bam*HI. The resulting 8.9 Kb pTSARib-PpyRE9H-TY1-  
157 tdTomato vector, containing a blasticidin S resistance cassette, was linearised with *Sph*I to  
158 integrate the rDNA promoter locus.

159 In order to generate the RED *L. major* strain, the same chimeric PpyRE9H/TY1/tdTomato  
160 protein coding sequence was amplified by PCR from the pTSARib-PpyRE9H-TY1-tdTomato  
161 vector. PCR product was cut with *Bgl*II and *Not*I restriction enzymes and ligated into the  
162 same sites of the pLEXSY-hyg2 expression vector (Jena Bioscience GmbH, Germany).

### 163 **2.3 Generation of the RED parasites**

164 Parasites genetically engineered to express the chimeric multiplex reporter protein  
165 PpyRE9H/TY1/tdTomato in their cytosol will be further referred as RED strains.

166 Trypanosomes BSF and PCF were transformed with an Amaxa Nucleofector (Lonza)  
167 (Burkard et al., 2007; MacGregor et al., 2013) and sub-cloned by limiting dilution. Clone  
168 selection was performed by measuring both bioluminescence in a microplate reader Infinite®  
169 200 (Tecan) and fluorescence with a Muse® cell Analyzer (Merck-Millipore). Cells were  
170 routinely counted with an automated Muse® cell Analyzer (Merck-Millipore) and / or manually  
171 with a KOVA hemocytometer according to the manufacturer's recommendations.

172 *L. major* promastigote parasites were transformed with the large *Swal* targeting fragment  
173 derived from the final 11.1 Kb pLEXY-PpyRE9H-TY1-tdTomato plasmid by electroporation  
174 and subsequent plating on semisolid media containing 200 µg/ml hygromycin B as previously  
175 described (Kapler et al., 1990). The fluorescent and bioluminescent clones were confirmed  
176 by using a microplate reader Infinite® 200 (Tecan) and a Muse® cell Analyzer (Merck-  
177 Millipore).

### 178 **2.4 In vitro fluorescence and bioluminescence quantification in RED parasites**

179 To perform the parasite density / fluorescence-bioluminescence intensity assay with the RED  
180 PCF and BSF trypanosomes, as well as with promastigotes of the RED *L. major* strain,  
181 parasites were counted, centrifuged and resuspended in fresh SDM-G, HMI-11 and M199  
182 medium, respectively. Then, 100µl (or 10<sup>7</sup> parasites) of this suspension were transferred into  
183 black clear-bottom 96-well plates and serial 2-fold dilutions were performed in triplicate  
184 adjusting the final volume to 200µl with 300 µg/ml of beetle luciferin (Promega, France).  
185 Luciferase activity was quantified after 10 minutes of incubation with a microplate reader  
186 Infinite® 200 (Tecan) or an IVIS® Spectrum imager (Perkin Elmer), following the instructions  
187 of the Promega Luciferase Assay System. After removal of intensity values from parasite-  
188 free medium corresponding to the background noise, results were analyzed as mean ±SD of  
189 three independent experiments.

### 190 **2.5 Tsetse fly maintenance, infection by RED *Trypanosoma brucei brucei* and** 191 **dissection**

192 *Glossina morsitans morsitans* tsetse flies were maintained in Roubaud cages at 24°C and  
193 60% hygrometry and fed through a silicone membrane with fresh mechanically defibrinated  
194 sheep blood. Teneral males (between 24h and 72h post-emergence) were allowed to ingest  
195 parasites in culture medium during their first meal through a silicone membrane. Here, we  
196 used either (i) cultured PCF trypanosomes at 5x10<sup>6</sup> cells per millilitre in SDM79 medium  
197 supplemented with 10% foetal bovine serum, 8mM glycerol and 10mM glutathione (MacLeod

198 et al., 2007), or (ii) freshly *in vitro* differentiated stumpy BSF trypanosomes resuspended at  
199  $2 \times 10^6$  cells per millilitre in SDMG medium supplemented with 10mM glutathione (MacLeod et  
200 al., 2007).

201 Flies were starved for at least 24 hours before being dissected. After rapid isolation of the  
202 salivary glands in a drop of phosphate buffer saline (PBS), whole tsetse alimentary tracts,  
203 from the distal part of the foregut to the malpighian tubules, were dissected and arranged  
204 lengthways in a another drop of PBS as previously described (Rotureau et al., 2011;  
205 Rotureau et al., 2012). Isolated organs were then either scrutinized under a microscope at  
206 high magnification and imaged, or individually dilacerated, dried on the slide and further  
207 treated for immuno-fluorescence (Rotureau et al., 2014).

208 Salivation tests were performed one month after the infective meal. First, cold-anesthetized  
209 flies were rapidly screened for the presence of a red fluorescent signal through the cuticle of  
210 their ventral abdomen under an epifluorescence M165FC stereomicroscope (Leica) at the  
211 10x magnification. Positive flies were sorted, starved for 48h, and individual flies were  
212 allowed to probe on warm clean glass slides for 5 minutes. Saliva drops were eventually  
213 checked for the presence of fluorescent metacyclic trypanosomes under a DMIL LED  
214 epifluorescence microscope (Leica) at the x60 magnification.

## 215 **2.6 Mouse strains and ethical statements**

216 Wild type BALB/c and C57BL/6J mice from Janvier Laboratory were used as models for  
217 experimental infection and monitoring of the bioluminescence with IVIS Spectrum and IVIS  
218 CT. In addition, to allow for further 3D intravital imaging of the lymphatic and blood systems,  
219 C57BL/6J-Fik1-EGFP mice expressing a GFP-tagged *Kdr (Flk1)* gene encoding the vascular  
220 endothelial growth factor receptor 2 (VEGFR-2), were also used (Ema et al., 2006). This  
221 study was conducted in strict accordance with the recommendations from the Guide for the  
222 Care and Use of Laboratory Animals of the European Union (European Directive  
223 2010/63/UE) and the French Government. The protocol was approved by the "Comité  
224 d'éthique en expérimentation animale de l'Institut Pasteur" CETEA 89 (Permit number: 2012-  
225 0043 and 2016-0017) and undertaken in compliance with Institut Pasteur Biosafety  
226 Committee (protocol CHSCT 12.131). BR is authorized to perform experiments on vertebrate  
227 animals (license #A-75-2035) and is responsible for all the experiments conducted personally  
228 or under his supervision.

## 229 **2.7 Mouse infections with RED parasites**

230 RED BSF ( $10^5$  parasites/mouse) were used to inoculate seven-week-old male C57BL/6J or  
231 BALB/c mice (Janvier, France) by the IP route. Parasitemia was assayed daily by automated  
232 fluorescent cell counting with a Muse cytometer (Merck-Millipore, detection limit at  $5 \times 10^2$

233 parasites/ml) according to the manufacturer's recommendations. Alternatively, mice were  
234 infected via the natural route, i.e. by infective bites: tsetse flies with a mature salivary gland  
235 infection, assessed by a salivation test, were individually allowed to bite on the belly of a  
236 naïve mouse for about 15 minutes, and blood absorption was further verified by examination  
237 of their abdomen.

238 Seven-week-old male BALB/c mice were injected with  $1 \times 10^6$  *L. major*  
239 PpyRE9H/TY1/tdTomato stationary-phase promastigotes (4 to 5-day old) in the hind  
240 footpads. After 4 weeks, animals were euthanized by cervical dislocation and popliteal lymph  
241 nodes were dissected for imaging. The total number of living parasites invading the target  
242 organs (popliteal lymph node draining the injected site) was calculated from serially-diluted  
243 single-cell suspensions and dispensed into 96-well plates. Parasitic load expressed as  
244 Limiting Dilution Assay Units (LDAU) after ten days of differentiation of amastigotes into  
245 promastigotes. The number of parasites was calculated as follows: Limit Dilution Assay Units  
246 (LDAU) = (geometric mean of titre from quadruplicate cultures) x (reciprocal fraction of the  
247 homogenized organ added to the first well). The titre was the reciprocal of the last dilution in  
248 which parasites were observed (Lima et al., 1997).

## 249 **2.8 Ex vivo fluorescence imaging of RED parasites**

250 For live fluorescence imaging of *Leishmania* promastigotes and all trypanosome stages,  
251 parasites in blood, in culture medium or isolated from tsetse fly midgut were observed either  
252 (i) with a DMI4000 microscope (Leica) and images were acquired with a Retiga-SRV camera  
253 (Q-Imaging), or (ii) with a DMIL LED microscope (Leica) and images were acquired with a  
254 digital color DFC450 C camera (Leica). Trypanosomes in tsetse organs were directly  
255 monitored with a M165FC stereomicroscope (Leica) with a monochromatic DFC30000 G  
256 camera (Leica). For intracellular *Leishmania* amastigote observations, peritoneal  
257 macrophages were collected from one BALB/c mouse. Then,  $5 \times 10^5$  cells were plated on Ibidi  
258 chambers and infected at a ratio of 10 stationary-phase promastigotes per macrophage as  
259 previously described, and maintained for 72h at 37°C in 5% CO<sub>2</sub> (Spath et al., 2000).  
260 Intracellular amastigotes were then observed with a DMI4000 microscope (Leica) and  
261 images were acquired with a Retiga-SRV camera (Q-Imaging). For figure preparation,  
262 specific ROI were selected and fluorescent frames were normalized to the same scale of  
263 intensity with ImageJ (NIH).

## 264 **2.9 In vivo fluorescence imaging of RED parasites**

265 RED trypanosomes were monitored in the ear of Kdr (Flk1) C57BL/6J Rj mice by spinning-  
266 disk confocal microscopy as described previously (Capewell et al., 2016). Briefly, mice were  
267 first anaesthetised by IP injection of ketamine (Imalgene 1000 at 125 mg/kg) and xylazine

268 (Rompun 2% at 12.5 mg/kg). Mice were wrapped in a heating blanket and placed on an  
269 aluminium platform with a central round opening of 21 mm in diameter. A coverslip was  
270 taped on the central hole and the mouse was positioned so that the ear was lying on this  
271 oiled coverslip. Imaging was performed using an UltraView ERS spinning-disk confocal  
272 system (Perkin Elmer) with a x40 oil objective (1.3 numerical aperture). Movies were  
273 acquired by an EM-CCD camera (Hamamatsu) controlled by the Volocity software (Perkin  
274 Elmer) with an exposure time of 500 ms for a total of 30 to 120 s. Images were analysed  
275 using ImageJ 1.48v and its plugin Bio-formats importer (NIH).

## 276 **2.10 *In vivo* bioluminescence imaging of RED parasites**

277 Infection by bioluminescent parasites was monitored daily by detecting the bioluminescence  
278 in whole animals with the IVIS® Spectrum imager (Perkin Elmer). The equipment consists of  
279 a cooled charge-coupled camera mounted on a light-tight chamber with a nose cone delivery  
280 device to keep the mice anaesthetized during image acquisition with 1.5% isoflurane. D-  
281 luciferin potassium salt (Promega) stock solution was prepared in PBS at 33.33 mg/ml, filter-  
282 sterilized and stored in a -20°C freezer. To produce bioluminescence, mice were inoculated  
283 IP with 150 µl of D-luciferin stock solution (250mg/kg). After 10 minutes of incubation to allow  
284 substrate dissemination, all mice were anaesthetized in an oxygen-rich induction chamber  
285 with 2% isoflurane, and images were acquired by using automatic exposure (30 seconds to 5  
286 minutes) depending on signal intensity. Images were analyzed with Living Image software  
287 version 4.3.1 (Perkin Elmer). Data were expressed in average radiance (p/s/cm<sup>2</sup>/sr)  
288 corresponding to the total flux of bioluminescent signal according to the selected area (total  
289 body of the mouse here). The background noise was removed by subtracting the  
290 bioluminescent / fluorescent signal of the control mouse from the infected ones for each  
291 acquisition.

292 Morphological / anatomical imaging technologies, such as computed tomography (CT) can  
293 be used to provide a combination of functional and anatomical data ensuring that maximum  
294 information is extracted from the infected animal model (Willmann et al., 2008). Longitudinal  
295 imaging is also used in pre-clinical studies to follow the progress of a disease or measure the  
296 effect of a therapeutic (Lim et al., 2011). Bioluminescence was acquired with a cooled CCD  
297 camera using the IVIS® Spectrum CT scanner (Perkin Elmer). Each animal was injected with  
298 150 mg/kg of D-luciferin IP 10 min prior to imaging. Six spectrally resolved images were  
299 acquired using emission filters at 560, 580, 600, 620, 640, and 660 nm with a bandwidth of  
300 20 nm each and an exposure time of 180 seconds. 3D tomographic reconstruction and  
301 superposition over the CT volume was performed using the DLIT algorithm available in the  
302 Living Image software 4.3. (Perkin Elmer), which uses single-view multispectral  
303 bioluminescence images to perform the reconstruction with segmentation of the CT images

304 in order to provide the mouse body boundary. The bioluminescence signal emitted by RED  
305 AnTat 1.1E parasites was monitored 4 days after the inoculation of  $10^5$  BSF by IP route in  
306 BALB/c mice.

### 307 **2.11 Immuno-fluorescence analysis and immuno-histology**

308 For immuno-histology, samples from the most bioluminescent skin regions were fixed in 4%  
309 paraformaldehyde over-night, processed into paraffin blocks and trimmed. Sections were  
310 processed for immuno-histochemical staining as described above. For immuno-fluorescence,  
311 parasites were settled on poly-L-lysine coated slides and fixed in methanol at  $-20^{\circ}\text{C}$  for 5  
312 seconds and re-hydrated in PBS for 10 minutes. Slides were incubated with the BB2 primary  
313 antibody diluted in PBS containing 0.1 % bovine serum albumin for 45 minutes at  $37^{\circ}\text{C}$ . The  
314 BB2 monoclonal antibody targets the Ty1-tag (mouse IgG1, up to 1/10) (Bastin et al., 1996).  
315 Slides were then washed and incubated with an anti-mouse-IgG1 secondary antibody  
316 coupled to Cy3 (Jackson) for 30 minutes at  $37^{\circ}\text{C}$ . Slides were finally stained with 4',6-  
317 diamidino-2-phenylindole (DAPI) for visualization of kinetoplast and nuclear DNA content,  
318 and mounted under cover slips with ProLong antifade reagent (Invitrogen), as previously  
319 described (Rotureau et al., 2011). Samples were observed either with a DMR microscope  
320 (Leica) and images were captured with a CoolSnap HQ camera (Roper Scientific), or with a  
321 DMI4000B microscope (Leica) and images were acquired with an ORCA-03G camera  
322 (Hamamatsu). Image acquisition was controlled using Micro-manager (NIH) and images  
323 were taken with the min/max threshold set at maximum.

### 324 **2.12 Western blotting**

325 For western blotting, samples were prepared by washing cells in serum-free medium before  
326 dilution with PBS and boiling in Laemmli for 5 minutes. SDS-PAGE separation was carried  
327 out after loading 10, 1 and 0.1  $\mu\text{g}$  of total proteins per lane (corresponding to  $10^6$ ,  $10^5$  and  
328  $10^4$  cells, respectively). Proteins were transferred onto polyvinylidene fluoride membranes for  
329 7 minutes by using the Trans-Blot<sup>®</sup> Turbo<sup>™</sup> technology (Bio-Rad), and blocked with 5%  
330 skimmed milk in PBS with 0.1% Tween 20 for 1 h prior to probing. The following primary  
331 antibodies were used by dilution in 2% milk in PBS with 0.1% Tween 20: L8C4 (non-diluted)  
332 (Kohl et al., 1999) and BB2 (1:50) (Bastin et al., 1996). Anti-mouse horseradish peroxidase-  
333 conjugated secondary antibodies (Amersham Biosciences) were used at a 1:20,000 dilution.  
334 Membranes were washed in PBS with 0.1% Tween 20 after blocking, between probing with  
335 primary and secondary antibodies and prior to band detection by chemiluminescence (GE  
336 healthcare).

337 **2.13 Measurements, normalization and statistical analysis**

338 Normalization of signals was carried out by parallel manipulation of min/max signals in  
339 ImageJ (NIH). For clarity purposes, brightness and contrast of several pictures were adjusted  
340 after their analysis in accordance with editorial policies. Statistical analyses and plots were  
341 performed with XLSTAT 2015.4.01 (Addinsoft) and Excel 2011 (Microsoft), respectively.  
342 Statistical analyses include linear regression analyses for bioluminescence / fluorescence  
343 intensity Vs. parasite density, ANOVA for growth curves, and ANCOVA for fly infection rates,  
344 with Tukey ad-hoc post-tests for inter-group comparison, all with 95% confidence.  
345

346 **3. Results**

347 We have generated a new chimeric triple reporter recombinant protein of 1,036 aa named  
348 PpyRE9H/TY1/tdTomato and composed by the fusion of (i) the human codon-optimized red-  
349 shifted version of the North American firefly *Photinus pyralis* luciferase (Branchini et al.,  
350 2005), (ii) a short amino acid sequence known as Ty1-tag (Bastin et al., 1996), and (iii) the  
351 tdTomato fluorescent protein (Fig. S1).

352 During the plasmid-construct amplification in *E. coli* DH5 $\alpha$ , the fusion protein expression was  
353 attested by the red colour of bacterial pellets and further confirmed under an epifluorescence  
354 microscope, demonstrating the potential usefulness of this construct also in prokaryotic cells.  
355 The triple reporter construct was then expressed in the cytoplasm of the eukaryotic protist  
356 parasites *Leishmania major* and *Trypanosoma brucei brucei*. These strains will be further  
357 referred to as the RED parasites in the entire article.

358 **3.1 In vitro and in vivo applications with RED *L. major* parasites**

359 In order to explore the usefulness of the novel triple reporter construct, a transgenic  
360 *Leishmania major* strain expressing the PpyRE9H/TY1/tdTomato was generated.  
361 Promastigotes of *L. major* Friedlin reference strain were electroporated and selected in semi-  
362 solid plates to obtain single fluorescent and bioluminescent clones. The presence of the  
363 construct was checked by PCR on genomic DNA (Fig. S2A-B). Parasites were scrutinized  
364 under an epifluorescence microscope and their fluorescence was compared to that of wild  
365 type cells (WT) (Fig. 1A-B). A strong and specific red fluorescent signal was homogenously  
366 distributed in both the cytoplasm and the flagellum of RED promastigote cells only, but it was  
367 absent from their nucleus. The fluorescence of RED cells was further confirmed at the  
368 population level by flow cytometry analysis (Fig. 1C-D). Moreover, parasite proliferation *in*  
369 *vitro* was comparable to that of the parental cell line (Fig. 1E).

370 A linear correlation was found between the number of cells and the emission of  
371 bioluminescence, by measuring the signal *in vitro* in 96-well plates with an IVIS Spectrum  
372 imager (Fig. 2A), being able to detect as few as 10<sup>3</sup> parasites (Fig. 2B). In parallel, this linear  
373 correlation was verified in a TECAN multiwell-plate reader for 5 RED sub-clones (Fig. 2C).  
374 Similarly, a linear correlation between the fluorescent signal intensity and the number of  
375 parasites was observed with both the imager (Fig. 2D), with a limit of detection at 10<sup>4</sup> cells  
376 (Fig. 2E), and the plate reader for 5 RED sub-clones (Fig. 2F).

377 To test the efficiency of the RED *L. major in vivo*, the virulence of the transfected parasites  
378 was firstly recovered by passing the strain once through BALB/c mice. In order to determine  
379 whether RED *L. major* parasites could be detected *in vivo* using whole-body imaging, 10<sup>6</sup>  
380 stationary-phase parasites were injected subcutaneously into the hind footpads of BALB/c

381 mice. Lesion progression was monitored both by the direct measurement of the  
382 bioluminescence (Fig. 3A) and fluorescence (Fig. 3B) emitted by RED amastigotes recorded  
383 in the IVIS Spectrum, and by the follow-up of the hind-limb lesions over four weeks (Fig. 3C-  
384 D). The bioluminescent signal start to increase from 5 days post-infection up to the end of the  
385 experiment, reaching a maximum radiance of  $6.3 \times 10^6$  p/s/cm<sup>2</sup>/sr after four weeks of infection.  
386 However, *in vivo* follow-up of the fluorescence during the infection course showed that the  
387 fluorescent signal was visible only from the 3<sup>rd</sup> week after the infection, leading to the  
388 expected conclusion that bioluminescence was much more sensitive to evaluate the  
389 progression of infection in this context (Fig. 3C-D). After 29 days, mice were sacrificed and  
390 the popliteal lymph nodes were extracted and imaged (Fig. 3E-F). Parasitic load (LDAU) in  
391 the popliteal lymph node draining the lesion of infected animals, determined by the limiting  
392 dilution method, was  $4.8 \times 10^6$  as an average of both infected organs per mouse. These  
393 results are in accordance with regular parasitic load experiments.  
394 Then, *in vitro* infection was performed in freshly collected resident peritoneal macrophages in  
395 order to allow parasites to differentiate into intracellular amastigotes forms in which the  
396 expression of the triple marker was confirmed as assessed by the presence of a specific red  
397 fluorescent signal (Fig. S3A).

### 398 **3.2 *In vitro* uses of RED *T. brucei* parasites**

399 In order to explore the usefulness of the novel triple reporter construct in another  
400 trypanosomatid parasite, transgenic *Trypanosoma brucei brucei* mammalian bloodstream  
401 forms (BSF) and insect procyclic forms (PCF) were transformed with the pTSARib-  
402 PpyRE9H-TY1-tdTomato vector and immediately sub-cloned by limiting dilution. The  
403 presence of the construct was checked by PCR on genomic DNA (Fig. S2). RED PCF  
404 trypanosomes in culture were scrutinized under a fluorescence microscope for a direct visual  
405 confirmation of their fluorescent phenotype as compared to WT cells. As expected, the triple  
406 reporter was homogenously distributed in the cytoplasm, and in a lesser extend in the  
407 flagellum, only in transformed parasites, but it was absent from their nucleus (Fig. 4A-B). The  
408 fluorescence of RED cells was further confirmed at the population level by flow cytometry  
409 analysis (Fig. 4C-D). Similar observations were done with RED BSF trypanosomes, yet with  
410 a lower overall fluorescence intensity as compared to that in RED PCF cells (Fig. 4E-H).  
411 Although the proliferation of PCF was significantly slower in transformed parasites compared  
412 to WT cells (doubling time of 14.5 h and 10.5 h, respectively, ANOVA  $p=0.034$ ) (Fig. 4I), the  
413 BSF proliferation rate *in vitro* was comparable to that of the parental cell line (doubling time  
414 of 6.5 h for both) (Fig. 4J).

415 First, in order to verify the reliability of the bioluminescent marker as well as to define its  
416 detection threshold, a parasite density / bioluminescence intensity analysis was performed in

417 96-micro-well plates with an IVIS Spectrum imager (Fig. 5A-B). Parasite density and  
418 bioluminescence intensity were correlated when bioluminescence levels were higher than  
419  $10^4$  p/s/cm<sup>2</sup>/sr, corresponding to about  $10^2$  RED BSF or RED PCF parasites, allowing  
420 estimation of the parasite density from *in vivo* imaging over this threshold (Fig. 5C). In  
421 parallel, this linear correlation was verified in a TECAN multiwell-plate reader for several  
422 RED sub-clones of both parasite stages (Fig. 5D-E), yet with some bioluminescence intensity  
423 level variations between clones, especially for RED PCF. Second, the fluorescent signal  
424 emitted by these RED *T. brucei* parasites was measured in a IVIS fluorescence reader and  
425 appeared to be correlated to their number in a dynamic range starting from  $10^3$  PCF and  $10^4$   
426 BSF (Fig. 5F-G), although the overall fluorescence intensity level in RED BSF was much  
427 lower compared to that in RED PCF (Fig. 5H). This is possibly due to the existence of BSF-  
428 specific chemical conditions in the cytosol, such as pH variations and / or high localized  
429 concentrations of cations, that may affect tdTomato activity, or to a higher photobleaching  
430 rate at 37°C, rather than to a lower turn-over or to a reduced folding efficiency, since the  
431 luciferase activity was not affected, as assessed by high bioluminescence levels. This  
432 observation was further confirmed by testing several subclones of both stages in a plate  
433 reader (Fig. 5I-J).

### 434 **3.3 *In vivo* uses of RED *T. brucei* parasites**

435 To test whether RED trypanosomes could be monitored *in vivo* in their insect vector,  
436 *Glossina morsitans morsitans* teneral males were experimentally infected with RED PCF  
437 parasites through a silicone membrane. One month after the infective meal, flies were  
438 screened under an epifluorescence binocular microscope for the presence of a specific red  
439 fluorescence through their abdominal cuticle, reflecting the presence of RED parasites in  
440 their midgut (Fig. 6A-B). To assess the stability of the triple reporter expression during the  
441 course of the infectious process, i.e. without any selective antibiotic pressure, both negative  
442 and positive flies were dissected and the presence of parasites in their midgut was verified  
443 by both light and epifluorescence microscope examination at a higher magnification (Fig. 6C-  
444 E). Living parasites were only detected in flies that were initially scored positive by  
445 fluorescence examination of the intact abdomen, demonstrating the stability of the triple  
446 reporter *in vivo* (Fig. 6F and Movie1). It is noteworthy that the red fluorescent component of  
447 the triple reporter could also be used to directly scrutinize the parasite development, motility  
448 and interactions *in vivo* or *ex vivo* within the tsetse host tissues and organs (Fig. 6E-F and  
449 Movie1) (Schuster et al., 2017). Then, in order to assess the virulence of RED parasites in  
450 the tsetse fly, a total of 17 batches of flies were fed with either WT BSF, WT PCF, RED BSF  
451 or RED PCF parasites in culture. Experimental infections were performed over a one-year  
452 period by comparing strains at least two by two. In total, 606 flies were dissected after one

453 month, and the infection rates in the midgut and salivary glands were compared between  
454 groups (Fig. 6G). For WT parasites, fly infection by BSF gave rise to significantly higher  
455 infection rates, especially in the midgut ( $p=0.019$ , ANOVA's Tukey ad-hoc post-test, 95%  
456 confidence). In total, RED parasites produced similar infection rates as compared to WT  
457 controls, except for the RED BSF that were significantly less prone than WT BSF to produce  
458 mature infection in the salivary glands ( $p=0.003$ , ANOVA's Tukey ad-hoc post-test, 95%  
459 confidence).

460 Conveniently, the possibility of assessing the infection by a simple observation of living flies  
461 allowed us to anticipate the number of flies which could be potentially infected at the salivary  
462 gland level. Therefore, in another experiment, only fluorescent flies were used for salivation  
463 tests one month after the infective meal in order to sort living tsetse flies with a mature  
464 salivary gland infection for further natural transmission experiments. Single flies with salivary  
465 gland infection were then used to naturally infect mice, and the course of the infection was  
466 monitored daily by acquiring the bioluminescent signal emitted by the parasites in the entire  
467 organism with an IVIS Spectrum imager (Fig. 7A). Mice bitten by uninfected flies and not  
468 bitten at all were used as controls. The parasitemia was also daily quantified by detecting  
469 RED fluorescent BSF in 5  $\mu$ l blood samples with a Muse bench flow-cytometer. In parallel,  
470 the parasitemia was verified by manual counting of living parasites with a KOVA  
471 hemocytometer (Fig. 7B). Similar parasitemia quantifications were obtained by both methods  
472 (not shown), demonstrating that the fluorescence, although being limited in RED BSF as  
473 compared to RED PCF, was stably maintained over the course of the infection. A significant  
474 bioluminescent signal was detected as soon as after 1 to 2 days and was persisting until the  
475 end of the experiment, whereas the parasitemia was only first detected after 17 days and  
476 further fluctuated by characteristic waves (Fig. 7C). This demonstrates that a substantial  
477 population of parasites remained extravascular during the entire course of the infection. As  
478 assessed by ventral and dorsal bioluminescence imaging, both the parasite distribution and  
479 density evolved in space and time during the entire infection course (Fig. 7C). This  
480 experiment reproduces our previous study where the bioluminescent signal intensity was  
481 used for quantifying the correlated parasite densities (Capewell et al., 2016). In the latter  
482 study, mice infected with RED BSF were sacrificed and dissected to record the  
483 bioluminescent signal in isolated organs: in contrast to the bioluminescent signals detected in  
484 the spleen, the liver, the inguinal and cervical lymph nodes and some adipose tissues, the  
485 skin was found to constitute the major anatomical reservoir of parasites even in the absence  
486 of detectable parasites in the blood (Capewell et al., 2016). Alternatively, in order to study the  
487 differential anatomical distribution of the RED parasites in living mice, we attempted to test  
488 longitudinal imaging with the IVIS Spectrum CT imager. The computed tomography  
489 application allowed us to extract the spatial 3D-localization of RED parasites, although only

490 in heavily infected organs (spleen, liver and lymph nodes) (Fig. 7D). To refine the  
491 observation of living parasites developing in the skin at the cell level, the same naturally-  
492 transmitted RED trypanosomes were also imaged *in vivo* using a spinning-disk confocal  
493 microscopy setting in the C57BL/6J-FIk1-EGFP mouse line that present green fluorescent  
494 endothelial cells in the lymphatic and blood vessels (Ema et al., 2006). Strikingly,  
495 extravascular trypanosomes were observed gliding and dividing in the dermal layer of the ear  
496 (Fig. S3B) (Capewell et al., 2016).

497 In total, the RED trypanosomes were comparable to the parental WT strain in terms of  
498 pleomorphism and tsetse infectivity. Both red markers were stably expressed in all stages of  
499 the parasite cycle, both *in vivo* and *in vitro*, in cells kept from 27°C to 37°C, in the absence of  
500 any antibiotic pressure, and over at least 3 months in total. All these features allowed us to  
501 scrutinize the kinetics of the same infection at different scales *in vivo* (single cells, tissue  
502 level and whole body).

### 503 **3.4 Immuno-detection of the triple reporter construct with the TY1 tag**

504 The bioluminescent and fluorescent properties of the two reporter proteins used in the  
505 construct mainly rely on their conformation and on the physico-chemical nature of the micro-  
506 environment. For this reason, common regular protocols, such as for electron microscopy,  
507 histology or protein biochemistry are known to at least partially alter protein structures, which  
508 results in a loss of enzymatic activity, fluorescence emission or immune-specificity. For these  
509 reasons, we have introduced the small Ty1-tag between the red-shifted luciferase and the  
510 tdTomato in order to stabilize the fusion protein and to serve as a third reporter in specific  
511 conditions where the two other reporters would not be detected. The Ty1-tag can be  
512 recognized by two different monoclonal antibodies with overlapping binding sites: BB2, which  
513 is an immunoglobulin G (IgG1) and TYG5, which is an immunoglobulin A.

514 The expression and accessibility of the Ty1 epitope was first assessed by  
515 immunofluorescence staining with BB2 in both RED *T. brucei* PCF (Fig. 8A) and RED *L.*  
516 *major* promastigotes (Fig. 8B) after a 5-seconds methanol fixation. The homogenous  
517 distribution of the signal within the entire cytoplasm and flagellum was similar to that obtained  
518 directly by recording the tdTomato emission in living cells (Fig.1B and 4B). Then, we  
519 performed a western blot in denaturing conditions in order to test the ability of BB2 to detect  
520 the Ty1 reporter in total protein samples from RED *T. brucei* PCF and RED *L. major*  
521 promastigote parasites (Fig. 8C). Different amounts of parasites ( $10^6$ ,  $10^5$  and  $10^4$ ) were  
522 tested in order to confirm the correlation between the total amount of proteins and the  
523 detection of the tag. A specific band of 110 kDa was revealed only in the protein samples  
524 from  $10^5$  and  $10^6$  transformed parasites. Finally, highly bioluminescent regions of the skin of  
525 naturally infected mice (Fig. 7A) were sampled, fixed in paraformaldehyde, paraffin-

526 embedded and treated for immuno-histological analysis with BB2. Although no direct red  
527 fluorescence was detected, probably as the result of the sample heating for paraffin-  
528 embedment, the BB2 antibody was able to *in situ* label skin-dwelling-parasites expressing  
529 the Ty1 tag (Fig. 8D). These results confirm the potential use of the Ty1-tag included in the  
530 chimeric triple reporter fusion protein in a wide variety of immunological assays pre-requiring  
531 chemical denaturation and / or heating of the samples.

## 532 **4 Discussion and conclusion**

### 533 **4.1 Importance of intravital imaging in research on trypanosomatids**

534 Intravital imaging approaches already led to important discoveries on the biology of  
535 trypanosomatid parasites. The use of bioluminescent *T. brucei* parasites has successively  
536 enable different research groups to identify specific anatomical niches that strongly support  
537 the preponderance of extravascular parasite populations during the infectious process. Claes  
538 and co-workers showed that parasites located in the testis were not cleared by trypanocidal  
539 drugs, as they were protected by the blood-testis barrier (Claes et al., 2009). Trindade *et al.*  
540 and Caljon *et al.* further observed a close association of *T. b. brucei* with adipocytes in fat  
541 tissues and subcutaneous adipose layers, respectively (Caljon et al., 2016; Trindade et al.,  
542 2016). At the same time, together with colleagues from Glasgow, Conakry and Kinshasa, we  
543 have demonstrated that the majority of *T. b. gambiense* parasites were actually rather  
544 developing in the extravascular matrix of the dermis of murine models, where they were seen  
545 actively swimming and dividing (Capewell et al., 2016). In another study by D'Archivio and  
546 co-workers, the importance of the late brain invasion by *T. vivax* parasites was assessed in a  
547 dynamic manner by intravital imaging of a bioluminescent strain (D'Archivio et al., 2013).  
548 Recently, the principal clinical, immunological and parasitological features associated with  
549 visceral leishmaniasis were characterized by *in vivo* imaging approaches of *L. donovani*  
550 transgenic parasites in a golden hamster model (Rouault et al., 2017) and the occurrence of  
551 multiple phases of brain invasion and inflammation was further unambiguously demonstrated  
552 (Melo et al., 2017). Bioluminescence has also been recently used to monitor the evolution of  
553 the *T. cruzi* parasite load in the digestive tract of its triatomine vector *Rhodnius prolixus* (Dias  
554 Fde et al., 2015).

555 Applied to drug development in high-throughput (HTS) *in vitro* assays as well as in *in vivo*  
556 murine models, bioluminescent and fluorescent trypanosomatid reporter strains have also  
557 proved their usefulness. Intravital multi-photon microscopy revealed that diminazene was  
558 unable to target *T. b. brucei* parasites that have already crossed the blood-brain barrier three  
559 weeks after the infection in a mouse model of stage 2 sleeping sickness (Myburgh et al.,  
560 2013). Reimão and co-workers evaluated the efficacy of miltefosine *in vivo* in a luciferase-

561 expressing *L. infantum chagasi* experimental model of infection in hamsters that mimics  
562 human disease (Reimao et al., 2015). A non-invasive model of lesion suppression has been  
563 recently validated for the semi-HTS screening of compounds against cutaneous  
564 leishmaniasis by using a bioluminescent strain of *L. major* (Caridha et al., 2017). Other  
565 studies have taken advantage of the use of fluorescent and / or bioluminescent parasites to  
566 screen myriads of compounds in multi-well plates. Annang and co-workers validated a HTS  
567 platform to screen a subset of microbial extracts against the 3 trypanosomatid-borne  
568 diseases in 384-well plates by using, among them, bioluminescent-*L. donovani* parasites  
569 (Annang et al., 2015). The use of *ex vivo* cultures from infected tissues or organs has been  
570 explored and exploited as well by some other research groups with bioluminescent *L.*  
571 *donovani* (Osorio et al., 2011) and *L. major* (Peniche et al., 2014), as well as with infrared-  
572 emitting *L. infantum* parasites (Calvo-Alvarez et al., 2015b).

#### 573 **4.2 Novel perspectives offered by the triple reporter**

574 Most of these studies are relying on the use of constructs encoding for single green  
575 fluorescent probes or single luciferases emitting in the green. This is not optimal for intravital  
576 imaging due to the high absorption of the light by the tissue components at these  
577 wavelengths, and this also limits the monitoring to a single scale, i.e. whole organism or  
578 tissue / cell level. To bypass this technical bias, we have simultaneously used two reporters  
579 stably producing light in the red wavelengths with a reduced absorption by tissues, resulted  
580 in an enhanced sensitivity of the monitoring, with equivalent detection thresholds compared  
581 to previous studies (Burrell-Saward et al., 2015; McLatchie et al., 2013; Taheri et al., 2015;  
582 Van Reet et al., 2014). In the present study, as in the one of McLatchie and colleagues  
583 (McLatchie et al., 2013), we used a human codon optimized *PpyRE9h* sequence that was  
584 adapted to *T. brucei*. However, although this would theoretically have not been optimal for  
585 *Leishmania*, whose genome are more GC-rich, our results demonstrate that this actually  
586 doesn't seem to affect the triple marker expression. Taheri and collaborators have monitored  
587 and tracked a cutaneous *Leishmania* infection in real time, by generating stably-transgenic *L.*  
588 *major* parasites that expressed a bi-reporter protein constituted by an EGFP fused to a firefly  
589 luciferase. They demonstrated that the simultaneous use of two reporters increases the  
590 experimental sensitivity for detection and quantification of parasites *in vitro* as well as during  
591 real-time infection in mice (Taheri et al., 2015). In the present work, the constitutive cytosolic  
592 expression of the red triple reporter in African trypanosome and *Leishmania* strains in mice  
593 allowed us to study the kinetics of the infection in the same animal and at different scales by  
594 successively using a combination of complementary imaging technologies. We have  
595 demonstrated the correct expression of the transgenic constructs with a clear correlation  
596 between the number of parasites and the bioluminescent / fluorescent signals *in vitro*, thus

597 permitting the estimation of the parasite load by means of signal acquisition. However, using  
598 this methodology for an exact *in vivo* quantification of the parasite densities in experimental  
599 host tissues will further require a higher degree of standardization and some more controls in  
600 order to obtain reliable and reproducible quantitative results. In total, the use of this triple  
601 reporter led us to access both qualitative and quantitative data on the development of RED *L.*  
602 *major* in a mouse model, as well as on the full parasite cycle of RED *T. brucei* in the tsetse  
603 digestive tract and in the mammalian host after natural transmission. Furthermore, the Ty1-  
604 tag was also used to refine the analysis of the same biological material after intravital  
605 imaging, by immuno-based approaches (western blot, immunofluorescence analyses,  
606 immunohistochemistry).

607 It was the powerful combination of both fluorescence and bioluminescence imaging that  
608 allowed us to recently formally prove that skin-dwelling parasites were readily ingested by  
609 tsetse flies to fulfil their parasite cycle (Capewell et al., 2016). In the context of other HAT  
610 research projects, the optimised triple reporter line described here would also possibly  
611 enhance the application of *in vivo* imaging to study stage II African trypanosomiasis in murine  
612 models. Indeed, it will provide a new framework for investigating host-parasite relationships,  
613 particularly in the context of CNS infections. In addition, it should be ideally suited to drug  
614 evaluation programmes. This RED triple reporter construct represents a powerful tool that  
615 could also be useful in many other fields of research where cellular model can be  
616 transformed. According to the plasmid vector used and to its way of integration, the signal  
617 intensities could theoretically be modulated. Moreover, although the size of the triple reporter  
618 is not exactly appropriated, one could think about its potential use for protein tagging.  
619 Possible simultaneous qualitative and quantitative applications in research are the use of its  
620 bioluminescence component for *in vitro* HTS drugs screening and *in vivo* monitoring  
621 (microbiology, immunology, parasitology, oncology, pharmacology, vaccinology...), the use  
622 of its fluorescence for *in vitro* assays (HTS drug screening, investigation of biological  
623 processes...) and *in vivo* monitoring (microbiology, immunology, parasitology, oncology...),  
624 and the use of the Ty1-tag for immuno-detection in fixed and treated samples after real-time  
625 intravital imaging.

626

627 **Conflict of interest statement**

628 The authors declare that the research was conducted in the absence of any commercial or  
629 financial relationships that could be construed as a potential conflict of interest.

630 **Author contribution statement**

631 ECA, CCT and AC contributed to the experiments.

632 ECA and BR contributed to study design, data analysis and manuscript writing.

633 **Funding statement**

634 This work was funded by the Institut Pasteur (PTR-403), by a French Government  
635 Investissement d’Avenir programme, Laboratoire d’Excellence “Integrative Biology of  
636 Emerging Infectious Diseases” (ANR-10-LABX-62-IBEID) and by the French National  
637 Agency for Scientific Research (Young Researcher Grant ANR-14-CE14-0019-01). ECA and  
638 CCT were funded by a French Government Investissement d’Avenir programme, Laboratoire  
639 d’Excellence “Integrative Biology of Emerging Infectious Diseases” (ANR-10-LABX-62-IBEID)  
640 and by the French National Agency for Scientific Research (Young Researcher Grant ANR-  
641 14-CE14-0019-01). AC and BR were funded by the Institut Pasteur.

642 **Acknowledgements**

643 We acknowledge Pascal Pescher and Gerald Späth, Keith Gull, Martin Taylor and Bruce  
644 Branchini for providing various reagents. We are grateful to Philippe Bastin for his strong  
645 human and scientific support. We especially thank Marie-Anne Nicola and Jean-Yves  
646 Tinevez from the Dynamic Imaging Platform, Imagopole, CiTech, at the Institut Pasteur, for  
647 their very efficient support in intravital imaging.

648 **Figure legends**

649 **Fig. 1: Fluorescence pattern and growth of the RED *L. major*.**

650 (A-B) Live epifluorescence microscopy images of a WT *L. major* promastigote (A) and a RED  
651 *L. major* promastigote (B) (normalized TdTomato fluorescence in red and DNA staining in  
652 blue). (C-D) Ungated flow-cytometry analysis profiles confirming the non-fluorescence and  
653 red fluorescence (in arbitrary units) of WT (C) and RED (D) *L. major* promastigote  
654 populations, respectively. (E) Growth profiles (mean  $\pm$  SD from triplicates) of RED *L. major*  
655 promastigotes (in red) compared to their parental WT strain (in blue).

656 **Fig. 2: Quantification of the RED *L. major* bioluminescence and fluorescence.**

657 Images of the bioluminescent (A) and fluorescent (D) signals emitted by serial 1/2 dilutions of  
658 RED *L. major* promastigotes observed with an IVIS Spectrum in a 96-well plate. The same  
659 analysis was performed in triplicates for the RED strain (lines RED 1 to RED3). An equivalent  
660 serial dilution of WT promastigotes was used as control (line WT). The last three wells  
661 containing only medium were used as blank (red square). Radiance intensity scales are  
662 provided in p/s/cm<sup>2</sup>/sr on the right of each picture. (B, E) The mean bioluminescent (B) and  
663 fluorescent (E) signals ( $\pm$  SD) emitted by RED promastigotes show a significant linear  
664 correlation with the number of cells (linear regression analysis;  $r^2=1.0$  with  $p<0.0001$  for BL;  
665  $r^2=0.99$  with  $p<0.0001$  for fluorescence). (C, F) Bioluminescent (C) and fluorescent (F)  
666 signals ( $\pm$  SD) emitted by 5 different RED *L. major* clones were measured in triplicates with a  
667 TECAN plate reader and plotted in arbitrary units (AU) according to the parasite density. A  
668 similar linear correlation was observed for all sub-clones.

669 **Fig. 3: *In vivo* imaging applications with the RED *L. major*.**

670 (A-B) *In vivo* whole-body images of BALB/c mice, including 1 uninfected control (C) and 4  
671 infected mice (1 to 4), acquired with an IVIS Spectrum imager. Bioluminescent (A) and  
672 fluorescent (B) signals acquired on the hind footpads 28 days post-infection. Radiance  
673 intensity scales are provided in p/s/cm<sup>2</sup>/sr under each picture. (C, D) Bioluminescent (C) and  
674 fluorescent (D) signals on the hind footpads were measured and plotted over the course of  
675 the infection. (E, F) RED *L. major* amastigotes residing in the popliteal draining lymph nodes  
676 of 2 mice dissected 4 weeks after inoculation emit bioluminescence (E) and fluorescence (F).  
677 Radiance intensity scales are provided in p/s/cm<sup>2</sup>/sr under each picture.

678 **Fig. 4: Fluorescence pattern and growth of the RED *T. brucei* PCF and BSF stages.**

679 (A-B and E-F) Live epifluorescence microscopy images of WT (A and E) and RED (B and F)  
680 *T. brucei* PCF (A-B) and BSF (E-F) (normalized TdTomato fluorescence in red and DNA  
681 staining in blue). (C-D and G-H) Ungated flow-cytometry analysis profiles confirming the non-

682 fluorescence and red fluorescence (in arbitrary unit) of WT (C and G) and RED (D and H) *T.*  
683 *brucei* PCF (C-D) and BSF (G-H) populations, respectively. (I-J) Growth profiles (mean  $\pm$  SD  
684 from triplicates) of WT (in blue) and RED (in red) *T. brucei* PCF (I) and BSF (J).

685 **Fig. 5: Bioluminescence and fluorescence quantification in the RED *T. brucei* PCF and**  
686 **BSF stages.**

687 Images of the bioluminescent (A-B) and fluorescent (F-G) signals emitted by serial 1/2  
688 dilutions of RED *T. b. brucei* PCF (A and F) and BSF (B and G) observed with an IVIS  
689 Spectrum in 96-well plates. The same analyses were performed in triplicates for the RED  
690 strains (lines RED 1 to RED3). An equivalent serial dilution of WT parasites was used as  
691 control (lines WT). The last three wells containing only medium were used as blank (red  
692 square). Radiance intensity scales are provided in p/s/cm<sup>2</sup>/sr on the right of each picture. (C  
693 and H) The mean bioluminescent (C) and fluorescent (H) signals ( $\pm$  SD) emitted by RED  
694 PCF (in blue, linear regression analysis with  $p < 0.0001$ ,  $r^2 = 0.97$  for BL and  $r^2 = 0.96$  for  
695 fluorescence) and RED BSF (in red, linear regression analysis with  $p < 0.0001$ ,  $r^2 = 0.87$  for BL  
696 and  $r^2 = 0.97$  for fluorescence) show a significant linear correlation with the number of cells.  
697 (D-E and I-J) Bioluminescent (D-E) and fluorescent (I-J) signals ( $\pm$  SD) emitted by 3 different  
698 RED *T. b. brucei* PCF sub-clones (D and I) and 4 different RED *T. b. brucei* BSF subclones  
699 (E and J) were measured in triplicates with a TECAN plate reader and plotted in arbitrary  
700 units (AU) according to the parasite density. A similar linear correlation was observed for all  
701 sub-clones.

702 **Fig. 6: Imaging applications with the RED *T. brucei* in the tsetse fly host.**

703 *Glossina morsitans morsitans* teneral males were fed with RED PCF and observed under an  
704 epifluorescence binocular microscope after one month in order to sort infected flies. A strong  
705 red fluorescent signal was observed through the ventral abdomen of infected flies (B) but not  
706 in non-infected flies (A). This was confirmed by dissection and observation of the fly midgut  
707 (C and D, respectively). Fluorescence was even detected dorsally in strongly infected flies  
708 (E), and individual RED parasites could be distinguished under the epifluorescence binocular  
709 microscope in and outside dissected midguts (F, still image from movie S1). (G) The  
710 virulence of RED parasites was assessed by feeding batches of tsetse flies with either WT  
711 BSF, WT PCF, RED BSF or RED PCF parasites resuspended in SDMG culture medium. The  
712 histogram shows the infection rates in the midgut and salivary glands observed one month  
713 post infection (\* statistically significant difference between indicated groups with  $p < 0.02$  by  
714 ANCOVA's Tukey ad-hoc post-test at 95% confidence).

715 **Fig. 7: Imaging applications with the RED *T. brucei* in the mammalian host after**  
716 **natural transmission.**

717 (A) *In vivo* whole-body images of C57BL/6J mice acquired with an IVIS Spectrum imager 8,  
718 15 and 22 days after a tsetse fly bite, including one mouse bitten an infected tsetse fly (+),  
719 one bitten by a non-infected fly (-) and one non-bitten (0). Radiance intensity scales are  
720 provided in p/s/cm<sup>2</sup>/sr. (B) Live RED BSF in a blood sample from mouse + (DNA in blue). (C)  
721 Total ventral (blue squares) and dorsal (green triangles) bioluminescent signals (total  
722 radiance in p/s/cm<sup>2</sup>/sr) were measured, normalized to negative controls and plotted over the  
723 course of the infection together with the parasitemia (red dots) for mouse +. (D)  
724 Bioluminescence and anatomical 3D computed tomography images acquired by an IVIS  
725 Spectrum CT on a BALB/c mouse 29 days post-inoculation. The 3D reconstruction view on  
726 the right panel has been decomposed in pictures along 3 distinct plans showed on the left  
727 (coronal in red, sagittal in blue and transaxial in green).

728 **Fig. 8: Detection of RED trypanosomatids with the Ty1-tag after sample alteration by**  
729 **specific treatments.**

730 (A, B) Immunofluorescence images of methanol-fixed RED *T. brucei* PCF (A) and RED *L.*  
731 *major* promastigotes (B) stained with the BB2 antibody (Ty1 in red) and DAPI (DNA in blue).  
732 (C) Reactivity of the BB2 monoclonal antibody against the Ty1-tag epitope (110 kDa) by  
733 Western Blot analysis. The L8C4 anti-PFR2 antibody (69 kDa) was used as a loading  
734 control. Total protein extracts from 10<sup>6</sup>, 10<sup>5</sup> and 10<sup>4</sup> cells were used to compare the  
735 expression levels of the Ty1-tag in RED *T. brucei* procyclic forms and RED *L. major*  
736 compared to their respective WT control strains. Ladders (L) are provided on both sides of  
737 the blot with their respective size in kDa. (D) Immuno-histological analysis of a paraffin-  
738 embedded bioluminescent skin section from a mouse infected with RED *T. brucei*, *in situ*  
739 stained with the BB2 antibody (Ty-1 in red) and DAPI (DNA in blue). A skin-dwelling-parasite  
740 expressing the Ty1-tag situated in the extracellular matrix of the dermis is indicated with a  
741 white arrow.

742 **Supplementary material**

743 **Fig. S1: The PpyRE9/TY1/tdTomato fusion protein.**

744 (A) Schematic view of the protein regions (1,036 aa). (B) DNA sequence (3,111 bp).

745 **Fig. S2: Detection of the *PpyRE9H/TY1/tdTomato*-encoding gene and integration**  
746 **strategies into genomic *RRNA* loci of *T. brucei* and *L. major*.**

747 (A) PCR analysis for confirmation of the genomic presence of the triple reporter sequence  
748 (primers 1/2) and the specific antibiotic cassettes in RED *T.brucei* (primers 3/4) and RED *L.*  
749 *major* (primers 5/6) parasites. (B) The upper scheme shows the final structure of the 18S  
750 *RRNA* locus of *T. brucei* with the planned integration of the triple marker sequence. The  
751 bottom scheme represents the expected integration of the chimeric 3.1 Kb multiplex reporter  
752 protein PpyRE9H/TY1/tdTomato in the genome of *L. major*. PARP SL: procyclin splice site;  
753 bsd: blasticidin resistance cassette; utr1: 5' untranslated region of *aprt* gene; utr2: 1.4 kb  
754 intergenic region from *cam* operon; and utr3: 5' UTR of *dhfr-ts* gene; hyg: hygromycin B  
755 resistance cassette. Primers 1 and 2 amplify the 3.1 Kb region of the PpyRE9H-TY1-  
756 tdTomato sequence (1-GGAGGACGCCAAGAACATCAAG; 2-  
757 TTACTIONGTACAGCTCGTCCATGC); primers 3 and 4 amplify the blasticidin antibiotic  
758 cassette (3-ATGGCCAAGCCTTTGTCTCAAG; 4-TTAGCCCTCCCACACATAACCAG); and  
759 primers 5 and 6 were used to amplify the hygromycin resistance cassette (5-  
760 ATGAAAAGCCTGAACTCACCGC; 6-CTATTCCTTTGCCCTCGGACG).

761 **Fig. S3: Further imaging applications with RED parasites to monitor host cell / parasite**  
762 **interactions at the cellular level.**

763 (A) RED *L. major* intracellular amastigotes within BALB/c peritoneal macrophages after 72 h  
764 of incubation (DNA in blue and red fluorescent amastigotes in red). (B) Still-image from a  
765 spinning-disk confocal microscope movie showing extravascular RED *T. brucei* parasites (in  
766 red) in the surrounding of a vascular or lymphatic vessel (in green) in the ear dermis of a  
767 living C57BL/6J-Flk1-EGFP mouse 21 days after an infective bite.

768 **Movie S1: RED *T. b. brucei* in the posterior midgut of a tsetse fly 7 days after the**  
769 **infective meal.**

770 Living RED *T. b. brucei* procyclic parasites observed with a binocular epifluorescence  
771 microscope within the posterior midgut of an infected tsetse fly 7 days after the infectious  
772 meal. Red fluorescent parasites can be seen swimming outside the organ.

773 **References**

- 774 Aksoy, S., Buscher, P., Lehane, M., Solano, P., Van Den Abbeele, J., 2017. Human African  
775 trypanosomiasis control: Achievements and challenges. *PLoS Negl Trop Dis* 11, e0005454.
- 776 Alvar, J., Velez, I.D., Bern, C., Herrero, M., Desjeux, P., Cano, J., Jannin, J., den Boer, M.,  
777 Team, W.H.O.L.C., 2012. Leishmaniasis worldwide and global estimates of its incidence.  
778 *PLoS One* 7, e35671.
- 779 Annang, F., Perez-Moreno, G., Garcia-Hernandez, R., Cordon-Obras, C., Martin, J., Tormo,  
780 J.R., Rodriguez, L., de Pedro, N., Gomez-Perez, V., Valente, M., Reyes, F., Genilloud, O.,  
781 Vicente, F., Castanys, S., Ruiz-Perez, L.M., Navarro, M., Gamarro, F., Gonzalez-  
782 Pacanowska, D., 2015. High-throughput screening platform for natural product-based drug  
783 discovery against 3 neglected tropical diseases: human African trypanosomiasis,  
784 leishmaniasis, and Chagas disease. *J Biomol Screen* 20, 82-91.
- 785 Barquilla, A., Saldivia, M., Diaz, R., Bart, J.M., Vidal, I., Calvo, E., Hall, M.N., Navarro, M.,  
786 2012. Third target of rapamycin complex negatively regulates development of quiescence in  
787 *Trypanosoma brucei*. *Proc Natl Acad Sci U S A* 109, 14399-14404.
- 788 Bastin, P., Bagherzadeh, Z., Matthews, K.R., Gull, K., 1996. A novel epitope tag system to  
789 study protein targeting and organelle biogenesis in *Trypanosoma brucei*. *Mol Biochem*  
790 *Parasitol* 77, 235-239.
- 791 Beattie, L., Kaye, P.M., 2011. Leishmania-host interactions: what has imaging taught us?  
792 *Cell Microbiol* 13, 1659-1667.
- 793 Branchini, B.R., Southworth, T.L., Khattak, N.F., Michelini, E., Roda, A., 2005. Red- and  
794 green-emitting firefly luciferase mutants for bioluminescent reporter applications. *Anal*  
795 *Biochem* 345, 140-148.
- 796 Brookman, J.L., Stott, A.J., Cheeseman, P.J., Burns, N.R., Adams, S.E., Kingsman, A.J.,  
797 Gull, K., 1995. An immunological analysis of Ty1 virus-like particle structure. *Virology* 207,  
798 59-67.
- 799 Brun, R., Schonenberger, 1979. Cultivation and in vitro cloning of procyclic culture forms of  
800 *Trypanosoma brucei* in a semi-defined medium. Short communication. *Acta Trop* 36, 289-  
801 292.
- 802 Burkard, G., Fragoso, C.M., Roditi, I., 2007. Highly efficient stable transformation of  
803 bloodstream forms of *Trypanosoma brucei*. *Mol Biochem Parasitol* 153, 220-223.
- 804 Burrell-Saward, H., Rodgers, J., Bradley, B., Croft, S.L., Ward, T.H., 2015. A sensitive and  
805 reproducible in vivo imaging mouse model for evaluation of drugs against late-stage human  
806 African trypanosomiasis. *The Journal of antimicrobial chemotherapy* 70, 510-517.
- 807 Buscher, P., Cecchi, G., Jamonneau, V., Priotto, G., 2017. Human African trypanosomiasis.  
808 *Lancet*.

809 Caljon, G., Van Reet, N., De Trez, C., Vermeersch, M., Perez-Morga, D., Van Den Abbeele,  
810 J., 2016. The Dermis as a Delivery Site of *Trypanosoma brucei* for Tsetse Flies. *PLoS*  
811 *Pathog* 12, e1005744.

812 Calvo-Alvarez, E., Alvarez-Velilla, R., Fernandez-Prada, C., Balana-Fouce, R., Reguera,  
813 R.M., 2015a. Trypanosomatids see the light: recent advances in bioimaging research. *Drug*  
814 *Discov Today* 20, 114-121.

815 Calvo-Alvarez, E., Stamatakis, K., Punzon, C., Alvarez-Velilla, R., Tejeria, A., Escudero-  
816 Martinez, J.M., Perez-Pertejo, Y., Fresno, M., Balana-Fouce, R., Reguera, R.M., 2015b.  
817 Infrared fluorescent imaging as a potent tool for in vitro, ex vivo and in vivo models of visceral  
818 leishmaniasis. *PLoS Negl Trop Dis* 9, e0003666.

819 Capewell, P., Cren-Travaille, C., Marchesi, F., Johnston, P., Clucas, C., Benson, R.A.,  
820 Gorman, T.A., Calvo-Alvarez, E., Crouzols, A., Jouvion, G., Jamonneau, V., Weir, W.,  
821 Stevenson, M.L., O'Neill, K., Cooper, A., Swar, N.K., Bucheton, B., Ngoyi, D.M., Garside, P.,  
822 Rotureau, B., MacLeod, A., 2016. The skin is a significant but overlooked anatomical  
823 reservoir for vector-borne African trypanosomes. *eLife* 5.

824 Caridha, D., Parriot, S., Hudson, T.H., Lang, T., Ngundam, F., Leed, S., Sena, J., Harris, M.,  
825 O'Neil, M., Sciotti, R., Read, L., Lecoeur, H., Hickman, M., Grogl, M., 2017. Use of Optical  
826 Imaging Technology in the Validation of a New, Rapid, Cost-Effective Drug Screen as Part of  
827 a Tiered In Vivo Screening Paradigm for Development of Drugs To Treat Cutaneous  
828 Leishmaniasis. *Antimicrob Agents Chemother* 61.

829 Carneiro, M.B., Hohman, L.S., Egen, J.G., Peters, N.C., 2017. Use of two-photon microscopy  
830 to study *Leishmania major* infection of the skin. *Methods*.

831 Claes, F., Vodnala, S.K., van Reet, N., Boucher, N., Lunden-Miguel, H., Baltz, T., Goddeeris,  
832 B.M., Buscher, P., Rottenberg, M.E., 2009. Bioluminescent imaging of *Trypanosoma brucei*  
833 shows preferential testis dissemination which may hamper drug efficacy in sleeping sickness.  
834 *PLoS Negl Trop Dis* 3, e486.

835 Coles, J.A., Stewart-Hutchinson, P.J., Myburgh, E., Brewer, J.M., 2017. The mouse cortical  
836 meninges are the site of immune responses to many different pathogens, and are accessible  
837 to intravital imaging. *Methods*.

838 Coombes, J.L., Robey, E.A., 2010. Dynamic imaging of host-pathogen interactions in vivo.  
839 *Nat Rev Immunol* 10, 353-364.

840 D'Archivio, S., Cosson, A., Medina, M., Lang, T., Minoprio, P., Goyard, S., 2013. Non-  
841 invasive in vivo study of the *Trypanosoma vivax* infectious process consolidates the brain  
842 commitment in late infections. *PLoS Negl Trop Dis* 7, e1976.

843 Dias Fde, A., Guerra, B., Vieira, L.R., Perdomo, H.D., Gandara, A.C., Amaral, R.J., Vollu,  
844 R.E., Gomes, S.A., Lara, F.A., Sorgine, M.H., Medei, E., de Oliveira, P.L., Salmon, D., 2015.  
845 Monitoring of the Parasite Load in the Digestive Tract of *Rhodnius prolixus* by Combined

846 qPCR Analysis and Imaging Techniques Provides New Insights into the Trypanosome Life  
847 Cycle. *PLoS Negl Trop Dis* 9, e0004186.

848 Dias, J.C., 2015. Evolution of Chagas disease screening programs and control programs:  
849 historical perspective. *Glob Heart* 10, 193-202.

850 Ema, M., Takahashi, S., Rossant, J., 2006. Deletion of the selection cassette, but not cis-  
851 acting elements, in targeted Flk1-lacZ allele reveals Flk1 expression in multipotent  
852 mesodermal progenitors. *Blood* 107, 111-117.

853 Forestier, C.L., 2013. Imaging host-Leishmania interactions: significance in visceral  
854 leishmaniasis. *Parasite Immunol* 35, 256-266.

855 Franco, J.R., Cecchi, G., Priotto, G., Paone, M., Diarra, A., Grout, L., Mattioli, R.C., Argaw,  
856 D., 2017. Monitoring the elimination of human African trypanosomiasis: Update to 2014.  
857 *PLoS Negl Trop Dis* 11, e0005585.

858 Gonzalez, U., Pinart, M., Sinclair, D., Firooz, A., Enk, C., Velez, I.D., Esterhuizen, T.M.,  
859 Tristan, M., Alvar, J., 2015. Vector and reservoir control for preventing leishmaniasis.  
860 *Cochrane Database Syst Rev*, CD008736.

861 Huet, D., Blisnick, T., Perrot, S., Bastin, P., 2014. The GTPase IFT27 is involved in both  
862 anterograde and retrograde intraflagellar transport. *eLife* 3, e02419.

863 Julkowska, D., Bastin, P., 2009. Tools for analyzing intraflagellar transport in trypanosomes.  
864 *Methods Cell Biol* 93, 59-80.

865 Kapler, G.M., Zhang, K., Beverley, S.M., 1990. Nuclease mapping and DNA sequence  
866 analysis of transcripts from the dihydrofolate reductase-thymidylate synthase (R) region of  
867 *Leishmania major*. *Nucleic Acids Res* 18, 6399-6408.

868 Kohl, L., Sherwin, T., Gull, K., 1999. Assembly of the paraflagellar rod and the flagellum  
869 attachment zone complex during the *Trypanosoma brucei* cell cycle. *J Eukaryot Microbiol* 46,  
870 105-109.

871 Kooy, R.F., Hirumi, H., Mooloo, S.K., Nantulya, V.M., Dukes, P., Van der Linden, P.M.,  
872 Duijndam, W.A., Janse, C.J., Overdulve, J.P., 1989. Evidence for diploidy in metacyclic  
873 forms of African trypanosomes. *Proc Natl Acad Sci U S A* 86, 5469-5472.

874 Lang, T., Lecoeur, H., Prina, E., 2009. Imaging *Leishmania* development in their host cells.  
875 *Trends Parasitol* 25, 464-473.

876 Le Ray, D., Barry, J.D., Easton, C., Vickerman, K., 1977. First tsetse fly transmission of the  
877 "AnTat" serodeme of *Trypanosoma brucei*. *Ann Soc Belg Med Trop* 57, 369-381.

878 Lewis, M.D., Francisco, A.F., Taylor, M.C., Kelly, J.M., 2015. A new experimental model for  
879 assessing drug efficacy against *Trypanosoma cruzi* infection based on highly sensitive in  
880 vivo imaging. *J Biomol Screen* 20, 36-43.

881 Lim, E., Modi, K., Christensen, A., Meganck, J., Oldfield, S., Zhang, N., 2011. Monitoring  
882 tumor metastases and osteolytic lesions with bioluminescence and micro CT imaging. *J Vis*  
883 *Exp*.

884 Lima, H.C., Bleyenbergh, J.A., Titus, R.G., 1997. A simple method for quantifying *Leishmania*  
885 in tissues of infected animals. *Parasitol Today* 13, 80-82.

886 Liu, H., Patel, M.R., Prescher, J.A., Patsialou, A., Qian, D., Lin, J., Wen, S., Chang, Y.F.,  
887 Bachmann, M.H., Shimono, Y., Dalerba, P., Adorno, M., Lobo, N., Bueno, J., Dirbas, F.M.,  
888 Goswami, S., Somlo, G., Condeelis, J., Contag, C.H., Gambhir, S.S., Clarke, M.F., 2010.  
889 Cancer stem cells from human breast tumors are involved in spontaneous metastases in  
890 orthotopic mouse models. *Proc Natl Acad Sci U S A* 107, 18115-18120.

891 MacGregor, P., Rojas, F., Dean, S., Matthews, K.R., 2013. Stable transformation of  
892 pleomorphic bloodstream form *Trypanosoma brucei*. *Mol Biochem Parasitol* 190, 60-62.

893 MacLean, L., Myburgh, E., Rodgers, J., Price, H.P., 2013. Imaging African trypanosomes.  
894 *Parasite Immunol* 35, 283-294.

895 MacLeod, E.T., Maudlin, I., Darby, A.C., Welburn, S.C., 2007. Antioxidants promote  
896 establishment of trypanosome infections in tsetse. *Parasitology* 134, 827-831.

897 Matlashewski, G., Arana, B., Kroeger, A., Be-Nazir, A., Mondal, D., Nabi, S.G., Banjara,  
898 M.R., Das, M.L., Marasini, B., Das, P., Medley, G., Satoskar, A., Nakhasi, H., Argaw, D.,  
899 Reeder, J., Olliaro, P., 2014. Research priorities for elimination of visceral leishmaniasis.  
900 *Lancet Glob Health* 2, e683-684.

901 McLatchie, A.P., Burrell-Saward, H., Myburgh, E., Lewis, M.D., Ward, T.H., Mottram, J.C.,  
902 Croft, S.L., Kelly, J.M., Taylor, M.C., 2013. Highly sensitive in vivo imaging of *Trypanosoma*  
903 *brucei* expressing "red-shifted" luciferase. *PLoS Negl Trop Dis* 7, e2571.

904 Melo, G.D., Goyard, S., Fiette, L., Boissonnas, A., Combadiere, C., Machado, G.F., Minoprio,  
905 P., Lang, T., 2017. Unveiling Cerebral Leishmaniasis: parasites and brain inflammation in  
906 *Leishmania donovani* infected mice. *Sci Rep* 7, 8454.

907 Mezzanotte, L., Blankevoort, V., Lowik, C.W., Kaijzel, E.L., 2014. A novel luciferase fusion  
908 protein for highly sensitive optical imaging: from single-cell analysis to in vivo whole-body  
909 bioluminescence imaging. *Analytical and bioanalytical chemistry* 406, 5727-5734.

910 Myburgh, E., Coles, J.A., Ritchie, R., Kennedy, P.G., McLatchie, A.P., Rodgers, J., Taylor,  
911 M.C., Barrett, M.P., Brewer, J.M., Mottram, J.C., 2013. In vivo imaging of trypanosome-brain  
912 interactions and development of a rapid screening test for drugs against CNS stage  
913 trypanosomiasis. *PLoS Negl Trop Dis* 7, e2384.

914 Ooi, C.P., Rotureau, B., Gribaldo, S., Georgikou, C., Julkowska, D., Blisnick, T., Perrot, S.,  
915 Subota, I., Bastin, P., 2015. The Flagellar Arginine Kinase in *Trypanosoma brucei* Is  
916 Important for Infection in Tsetse Flies. *PLoS ONE* 10, e0133676.

917 Osorio, Y., Travi, B.L., Renslo, A.R., Peniche, A.G., Melby, P.C., 2011. Identification of small  
918 molecule lead compounds for visceral leishmaniasis using a novel ex vivo splenic explant  
919 model system. *PLoS Negl Trop Dis* 5, e962.

920 Patel, M.R., Chang, Y.F., Chen, I.Y., Bachmann, M.H., Yan, X., Contag, C.H., Gambhir, S.S.,  
921 2010. Longitudinal, noninvasive imaging of T-cell effector function and proliferation in living  
922 subjects. *Cancer Res* 70, 10141-10149.

923 Peniche, A.G., Osorio, Y., Renslo, A.R., Frantz, D.E., Melby, P.C., Travi, B.L., 2014.  
924 Development of an ex vivo lymph node explant model for identification of novel molecules  
925 active against *Leishmania major*. *Antimicrob Agents Chemother* 58, 78-87.

926 Perez-Molina, J.A., Molina, I., 2017. Chagas disease. *Lancet*.

927 Reimao, J.Q., Oliveira, J.C., Trinconi, C.T., Cotrim, P.C., Coelho, A.C., Uliana, S.R., 2015.  
928 Generation of luciferase-expressing *Leishmania infantum chagasi* and assessment of  
929 miltefosine efficacy in infected hamsters through bioimaging. *PLoS Negl Trop Dis* 9,  
930 e0003556.

931 Reithinger, R., Dujardin, J.C., Louzir, H., Pirmez, C., Alexander, B., Brooker, S., 2007.  
932 Cutaneous leishmaniasis. *Lancet Infect Dis* 7, 581-596.

933 Rotureau, B., Ooi, C.P., Huet, D., Perrot, S., Bastin, P., 2014. Forward motility is essential for  
934 trypanosome infection in the tsetse fly. *Cell Microbiol* 16, 425-433.

935 Rotureau, B., Subota, I., Bastin, P., 2011. Molecular bases of cytoskeleton plasticity during  
936 the *Trypanosoma brucei* parasite cycle. *Cell Microbiol* 13, 705-716.

937 Rotureau, B., Subota, I., Buisson, J., Bastin, P., 2012. A new asymmetric division contributes  
938 to the continuous production of infective trypanosomes in the tsetse fly. *Development* 139,  
939 1842-1850.

940 Rotureau, B., Van Den Abbeele, J., 2013. Through the dark continent: African trypanosome  
941 development in the tsetse fly. *Frontiers in cellular and infection microbiology* 3, 53.

942 Rouault, E., Lecoœur, H., Meriem, A.B., Minoprio, P., Goyard, S., Lang, T., 2017. Imaging  
943 visceral leishmaniasis in real time with golden hamster model: Monitoring the parasite burden  
944 and hamster transcripts to further characterize the immunological responses of the host.  
945 *Parasitol Int* 66, 933-939.

946 Schuster, S., Kruger, T., Subota, I., Thusek, S., Rotureau, B., Beilhack, A., Engstler, M.,  
947 2017. Developmental adaptations of trypanosome motility to the tsetse fly host environments  
948 unravel a multifaceted in vivo microswimmer system. *eLife* 6.

949 Spath, G.F., Epstein, L., Leader, B., Singer, S.M., Avila, H.A., Turco, S.J., Beverley, S.M.,  
950 2000. Lipophosphoglycan is a virulence factor distinct from related glycoconjugates in the  
951 protozoan parasite *Leishmania major*. *Proc Natl Acad Sci U S A* 97, 9258-9263.

952 Stanaway, J.D., Roth, G., 2015. The burden of Chagas disease: estimates and challenges.  
953 *Glob Heart* 10, 139-144.

954 Taheri, T., Saberi Nik, H., Seyed, N., Doustdari, F., Etemadzadeh, M.H., Torkashvand, F.,  
955 Rafati, S., 2015. Generation of stable *L. major*(+EGFP-LUC) and simultaneous comparison  
956 between EGFP and luciferase sensitivity. *Exp Parasitol* 150, 44-55.

957 Takai, A., Nakano, M., Saito, K., Haruno, R., Watanabe, T.M., Ohyanagi, T., Jin, T., Okada,  
958 Y., Nagai, T., 2015. Expanded palette of Nano-lanterns for real-time multicolor luminescence  
959 imaging. *Proc Natl Acad Sci U S A* 112, 4352-4356.

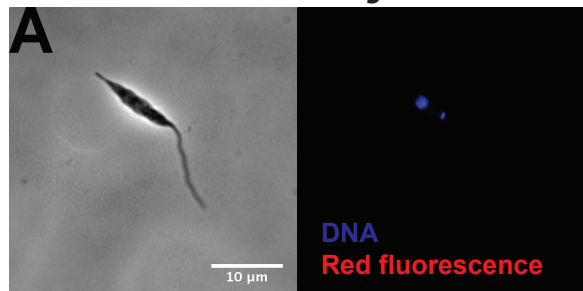
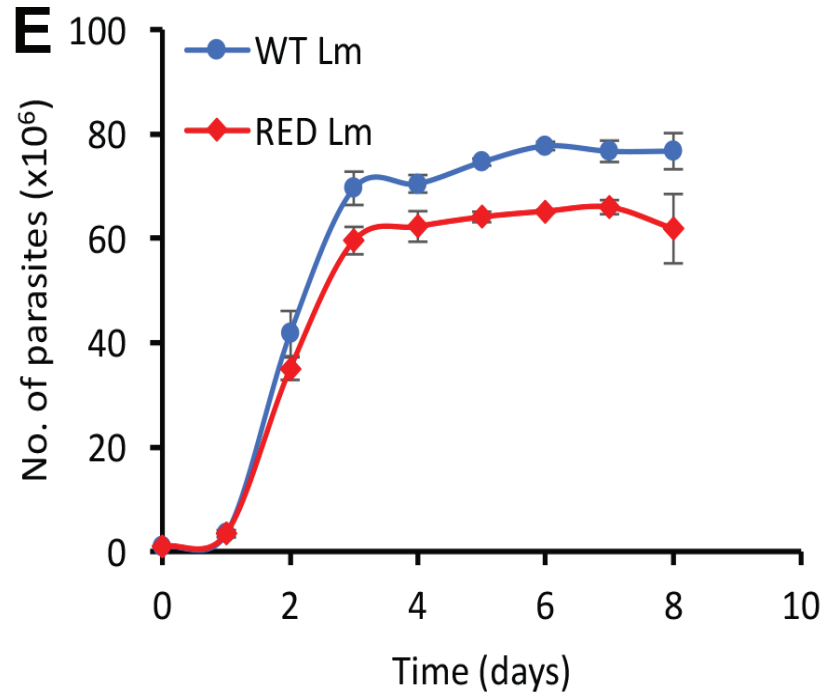
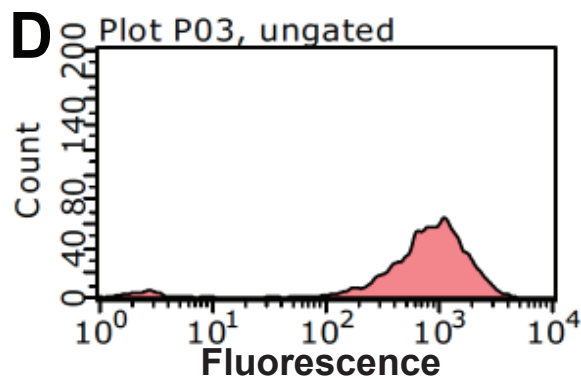
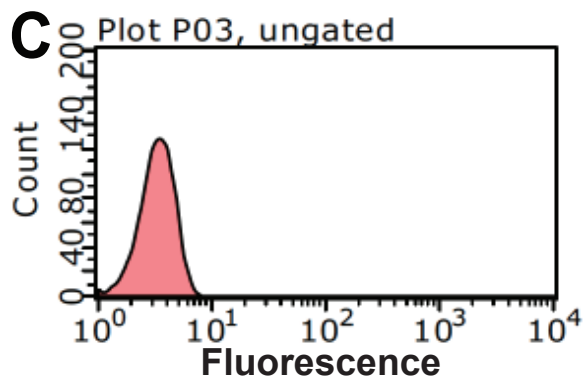
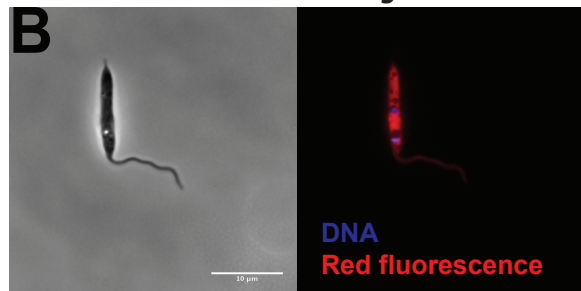
960 Trindade, S., Rijo-Ferreira, F., Carvalho, T., Pinto-Neves, D., Guegan, F., Aresta-Branco, F.,  
961 Bento, F., Young, S.A., Pinto, A., Van Den Abbeele, J., Ribeiro, R.M., Dias, S., Smith, T.K.,  
962 Figueiredo, L.M., 2016. *Trypanosoma brucei* Parasites Occupy and Functionally Adapt to the  
963 Adipose Tissue in Mice. *Cell Host Microbe*.

964 Van Reet, N., Van de Vyver, H., Pyana, P.P., Van der Linden, A.M., Buscher, P., 2014. A  
965 panel of *Trypanosoma brucei* strains tagged with blue and red-shifted luciferases for  
966 bioluminescent imaging in murine infection models. *PLoS Negl Trop Dis* 8, e3054.

967 Willmann, J.K., van Bruggen, N., Dinkelborg, L.M., Gambhir, S.S., 2008. Molecular imaging  
968 in drug development. *Nat Rev Drug Discov* 7, 591-607.

969 Xong, H.V., Vanhamme, L., Chamekh, M., Chimfwembe, C.E., Van Den Abbeele, J., Pays,  
970 A., Van Meirvenne, N., Hamers, R., De Baetselier, P., Pays, E., 1998. A VSG expression  
971 site-associated gene confers resistance to human serum in *Trypanosoma rhodesiense*. *Cell*  
972 95, 839-846.

973

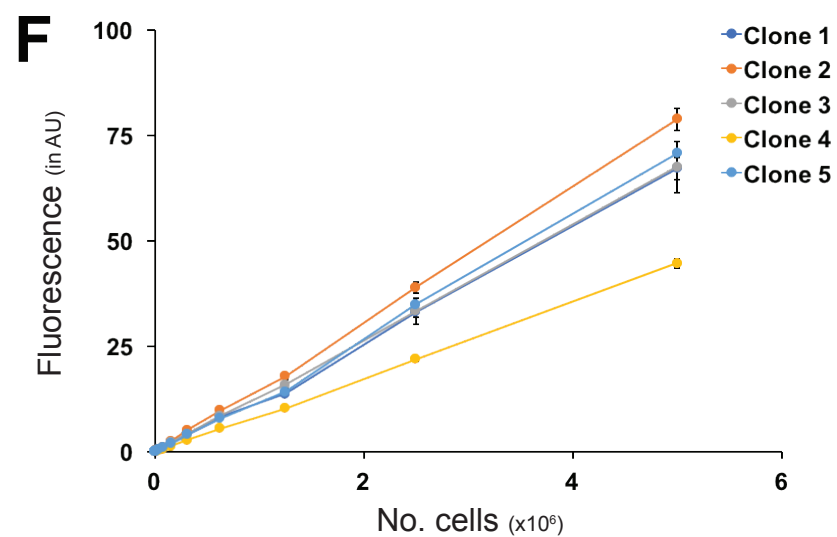
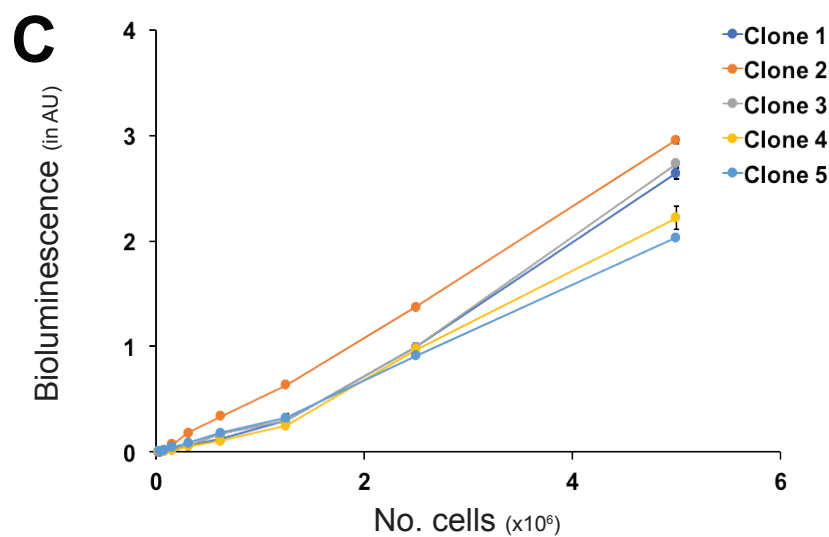
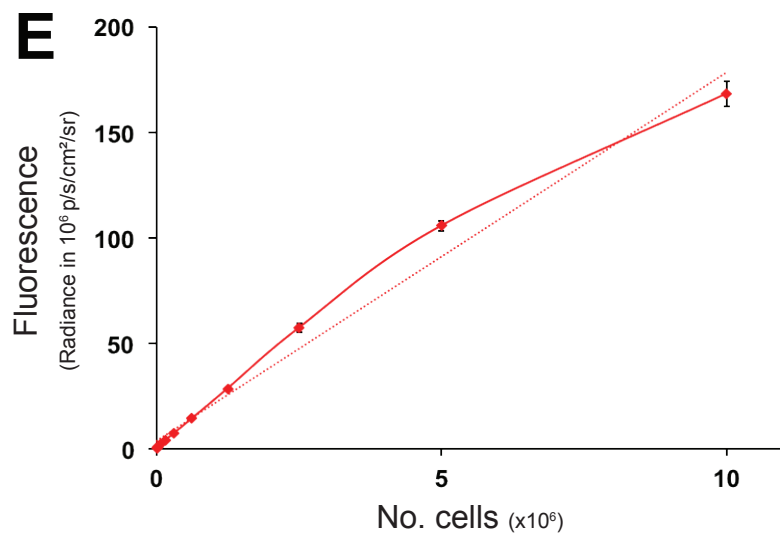
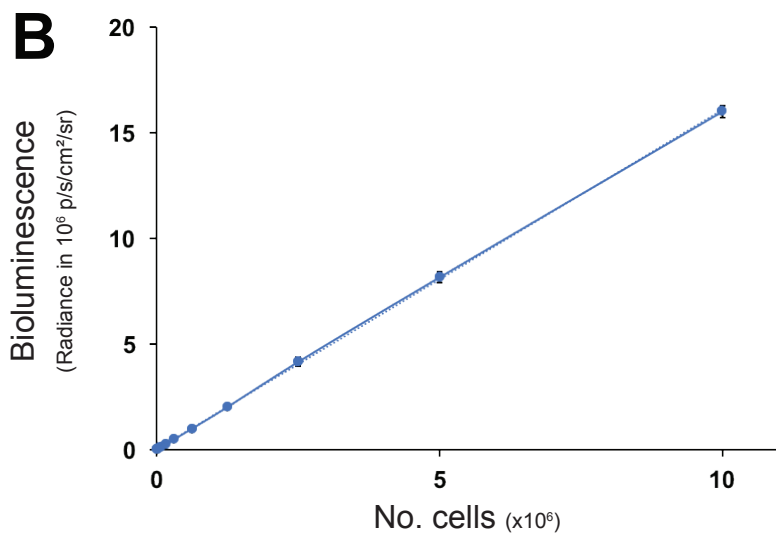
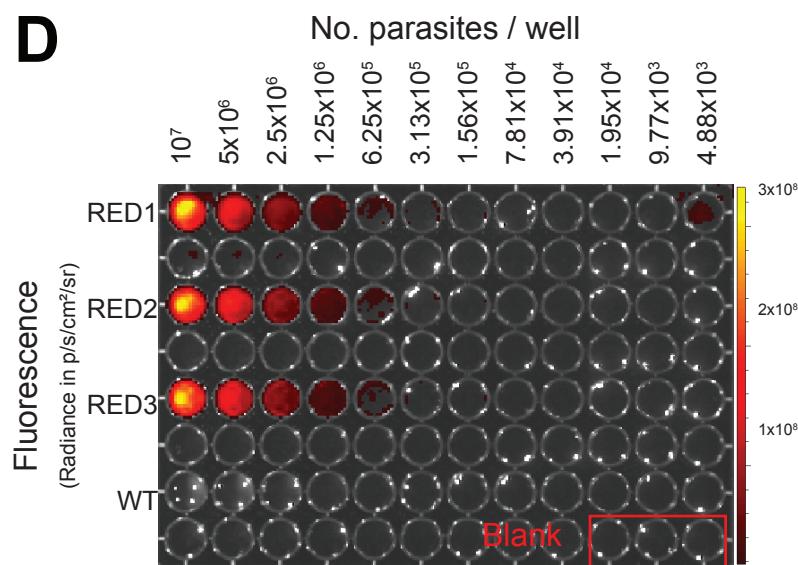
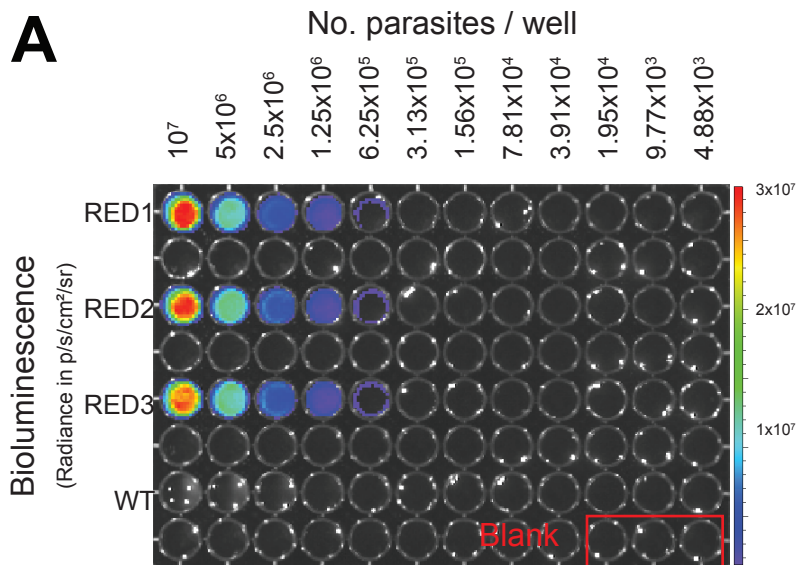
**WT *L. major*****RED *L. major***

# Bioluminescence

(Radiance in p/s/cm<sup>2</sup>/sr)

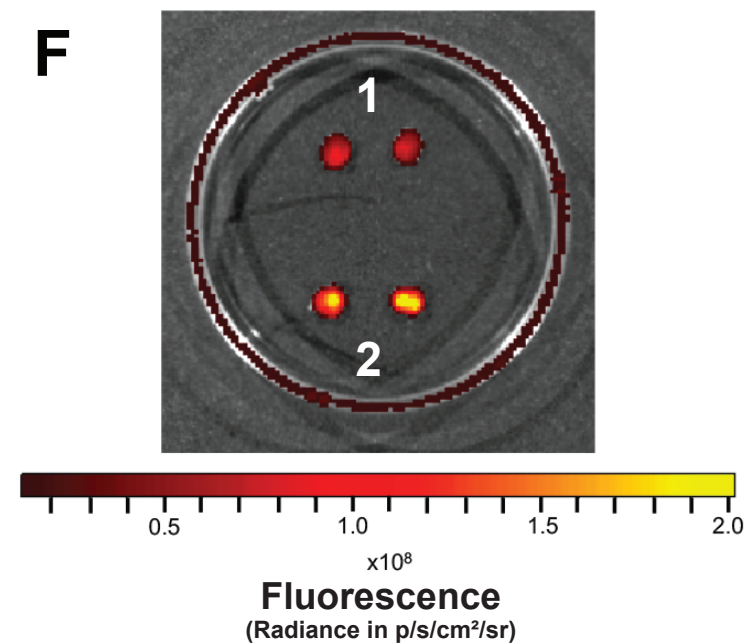
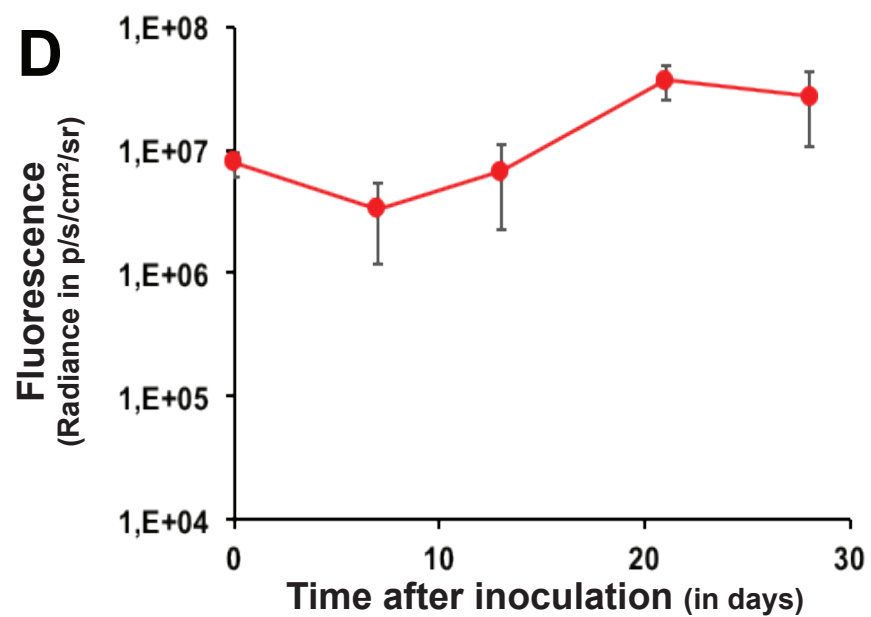
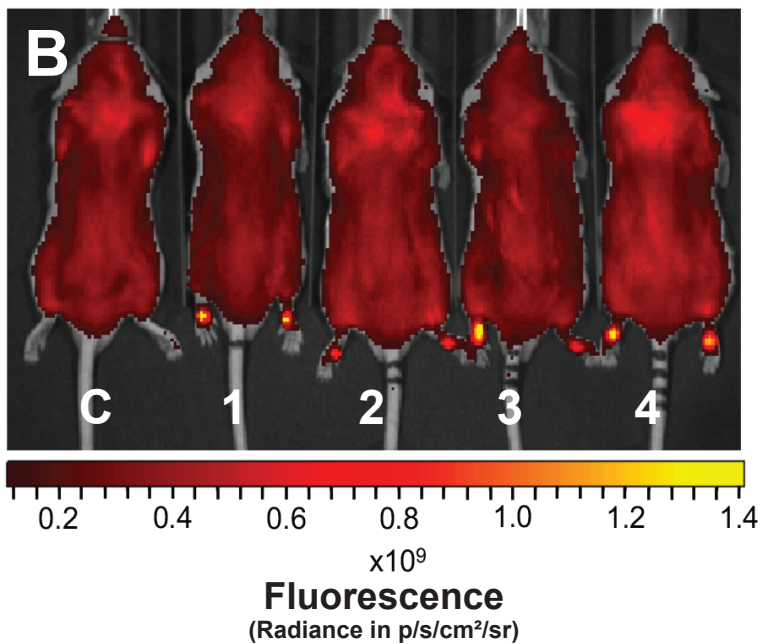
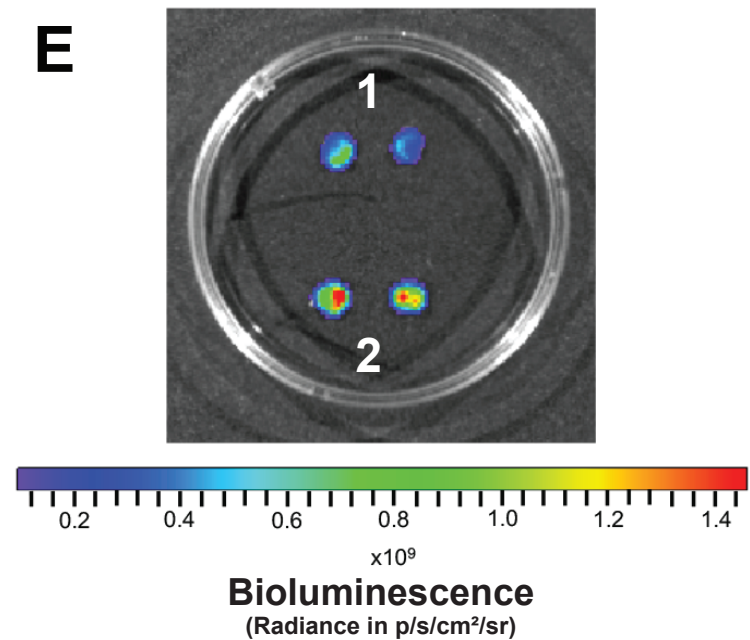
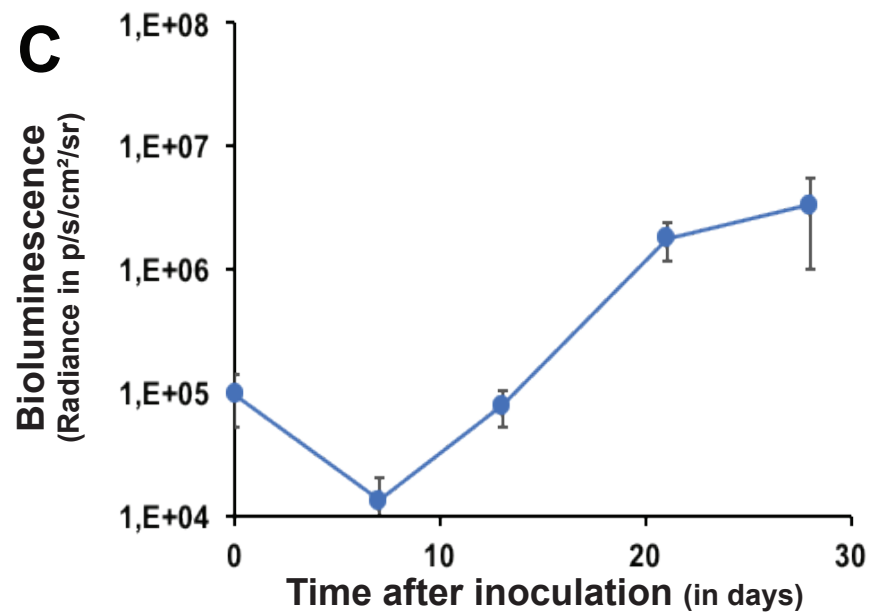
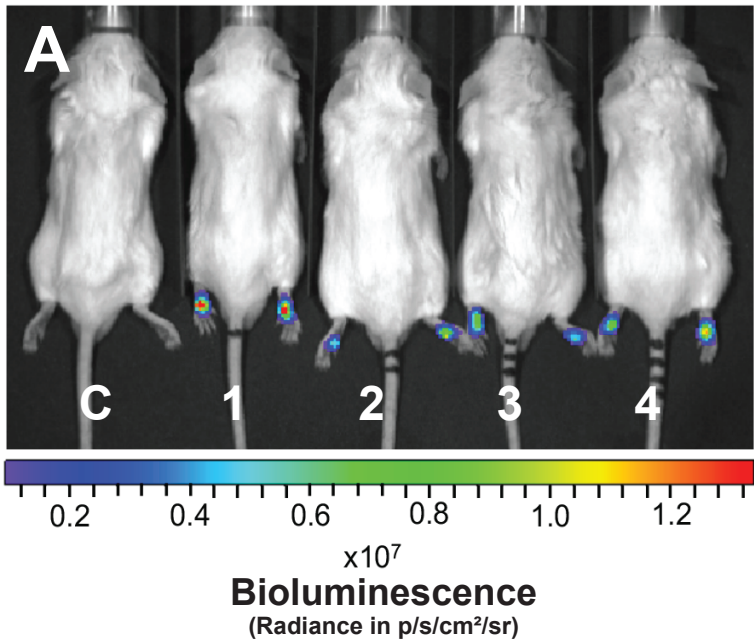
# Fluorescence

(Radiance in p/s/cm<sup>2</sup>/sr)



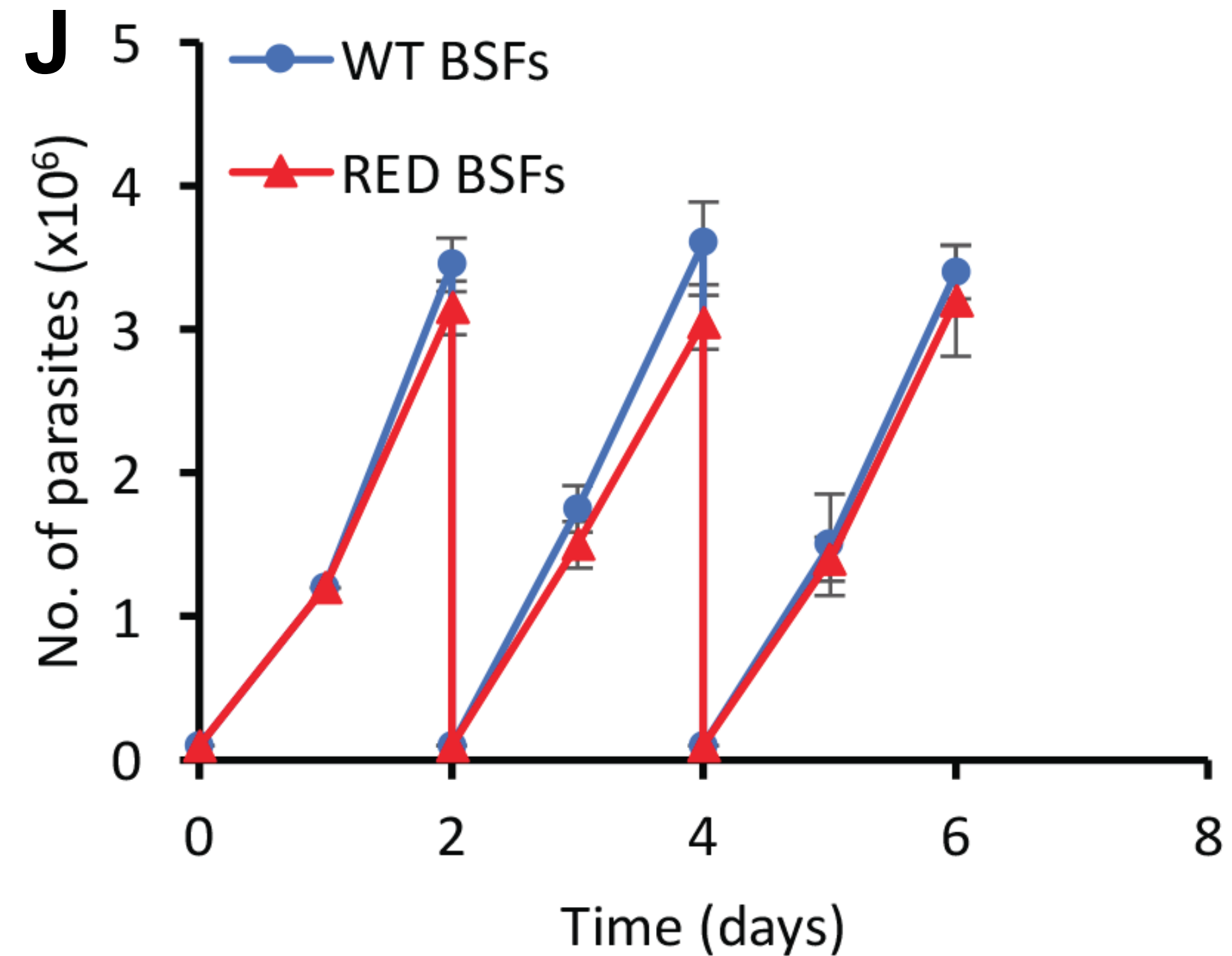
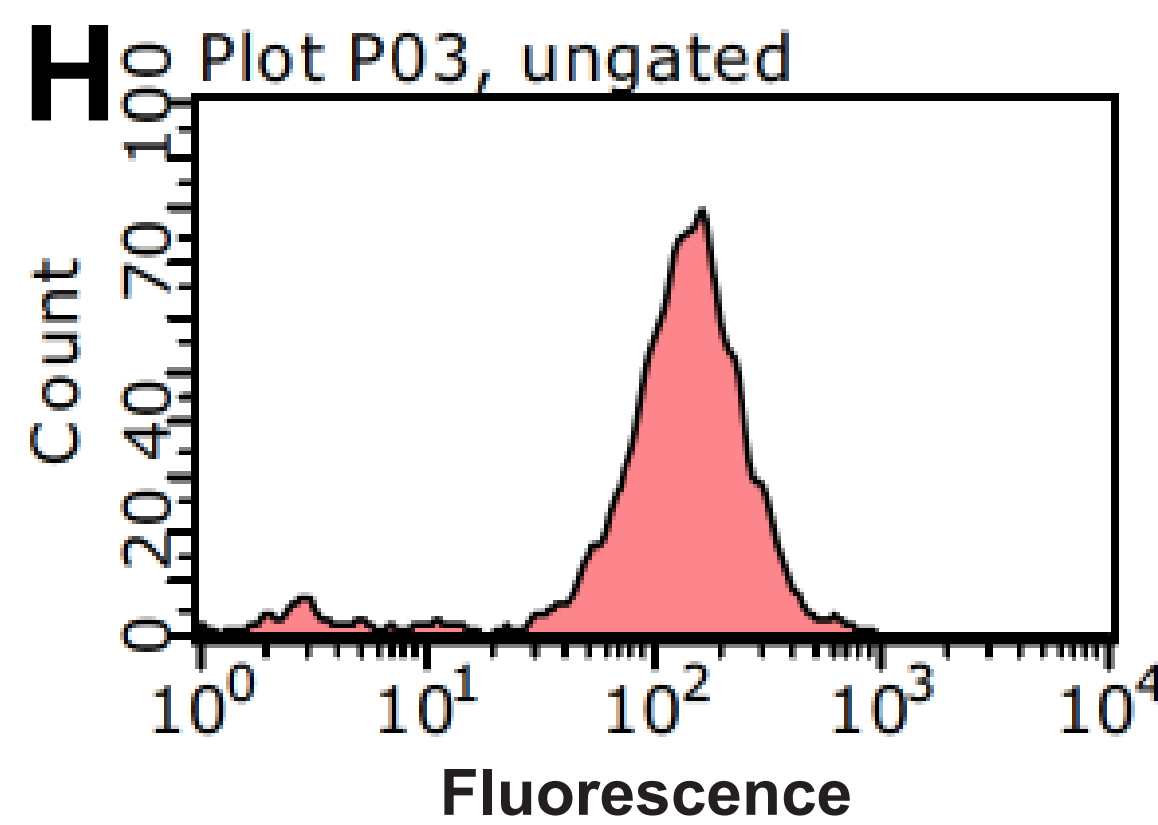
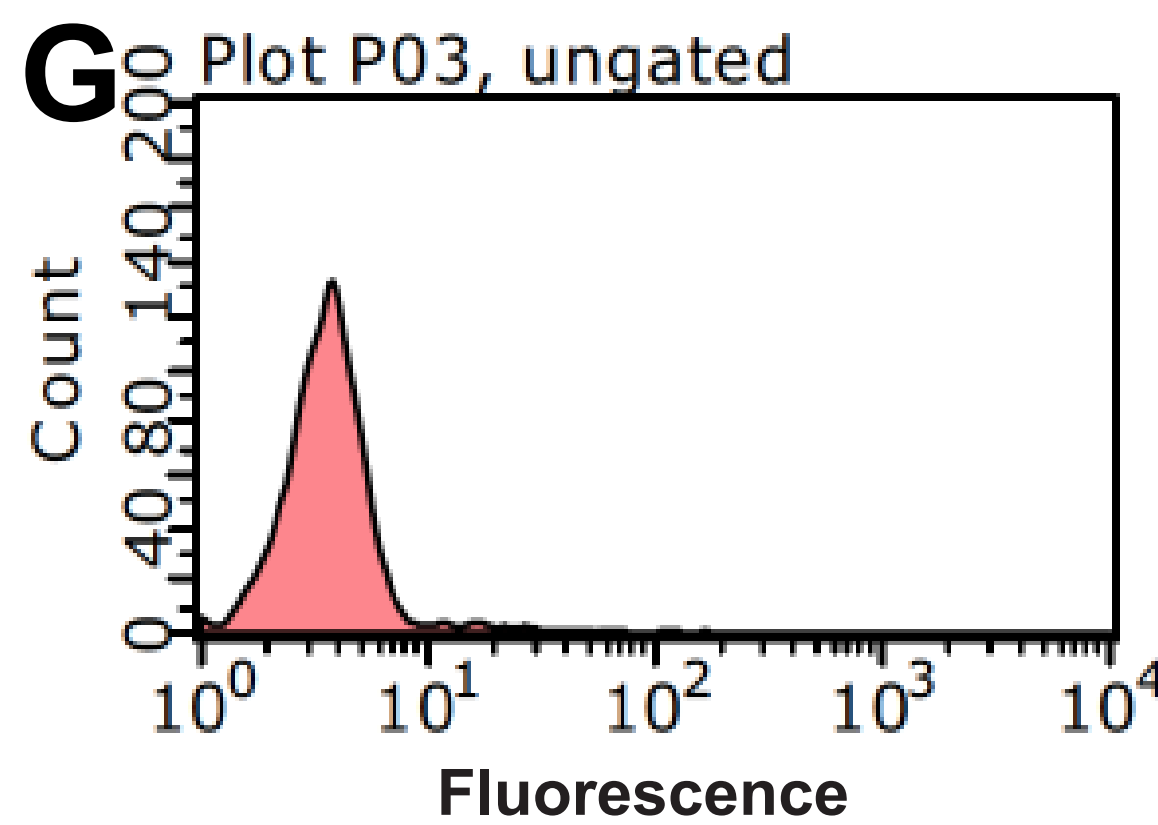
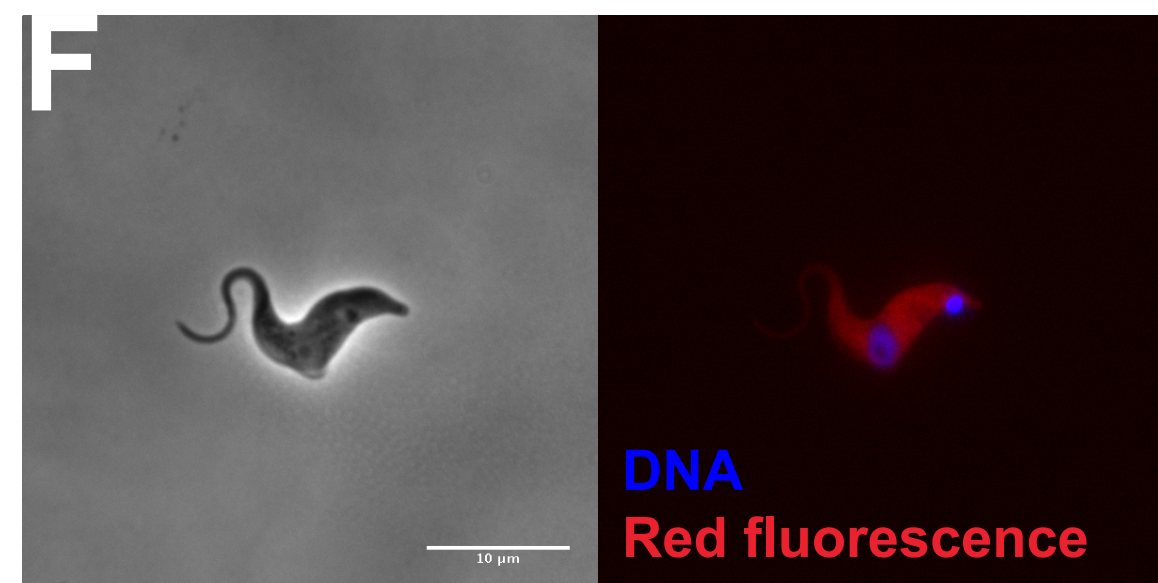
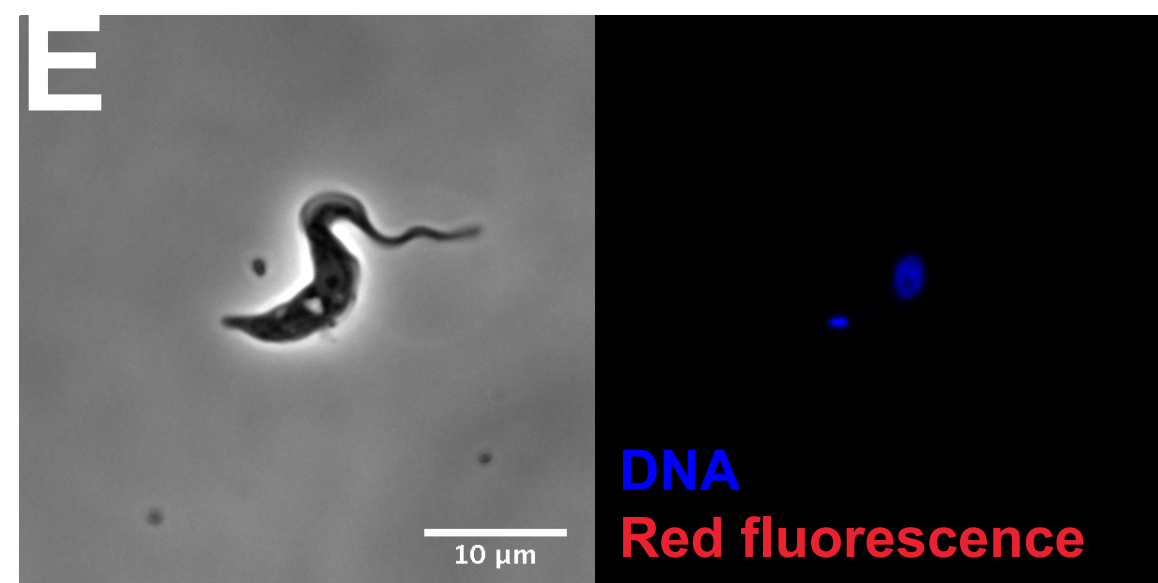
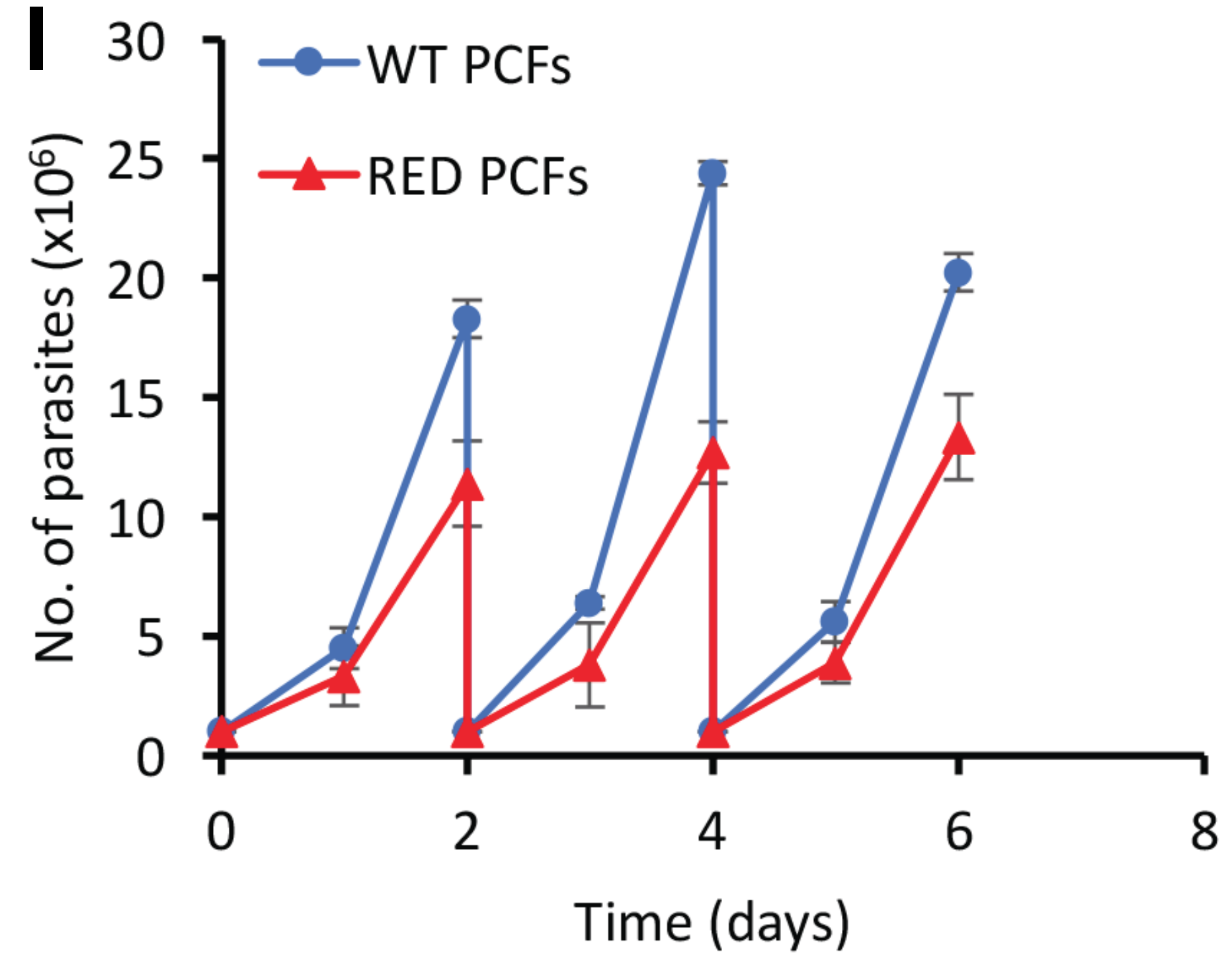
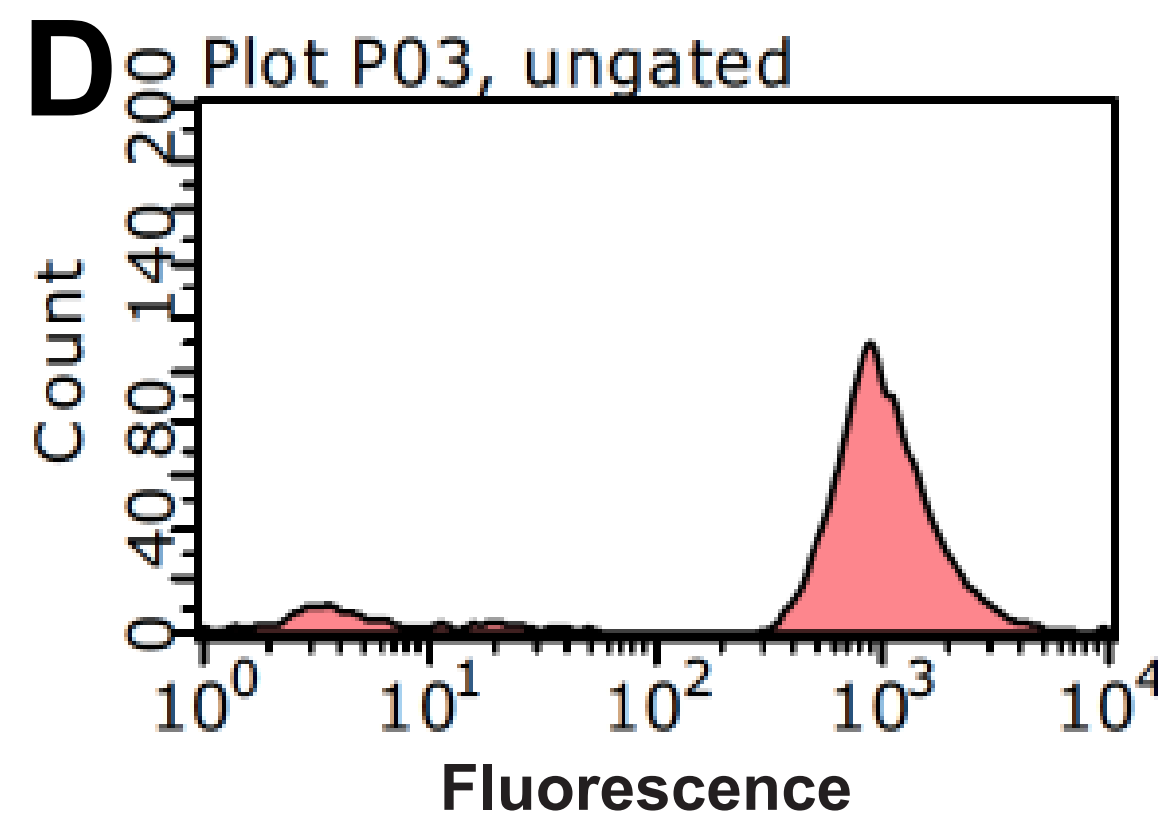
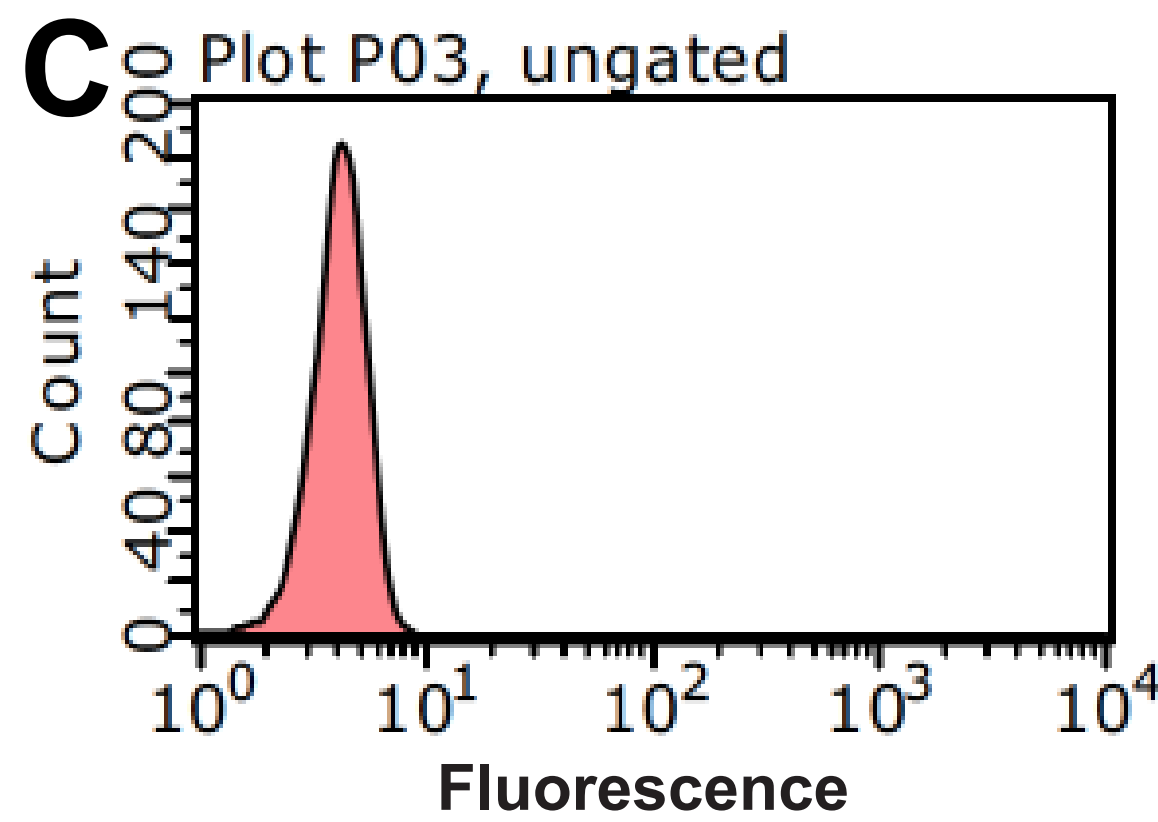
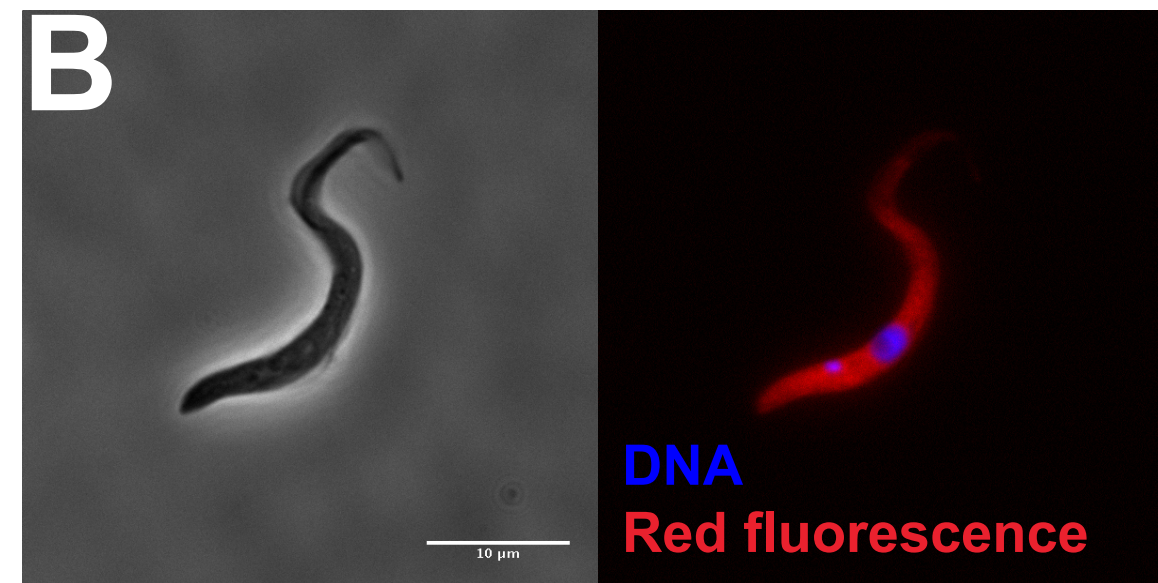
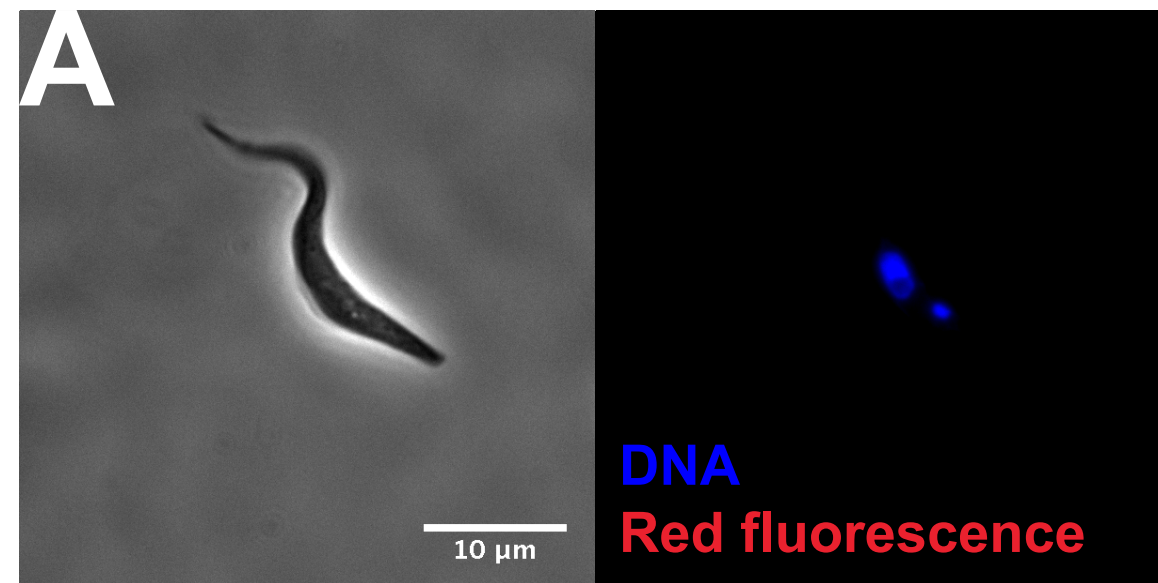
Imager

Plate reader



# WT *T. b. brucei*

# RED *T. b. brucei*



# Bioluminescence

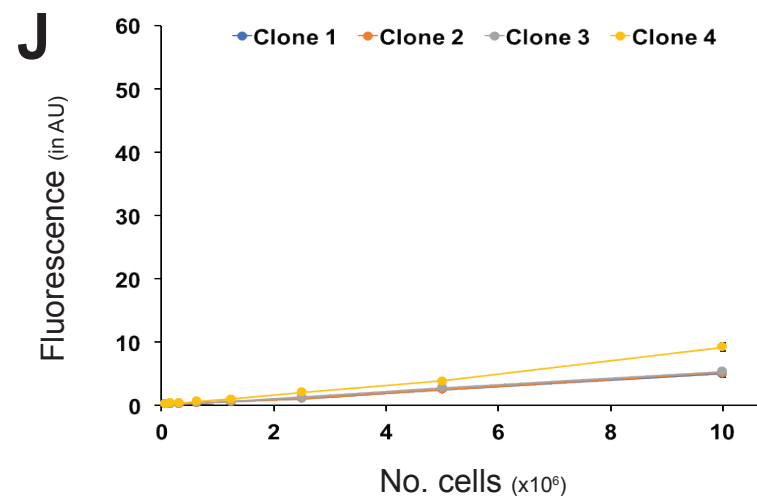
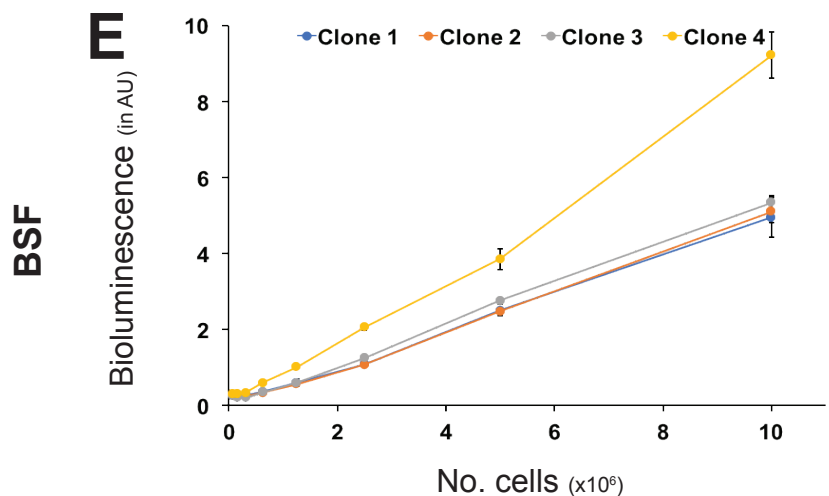
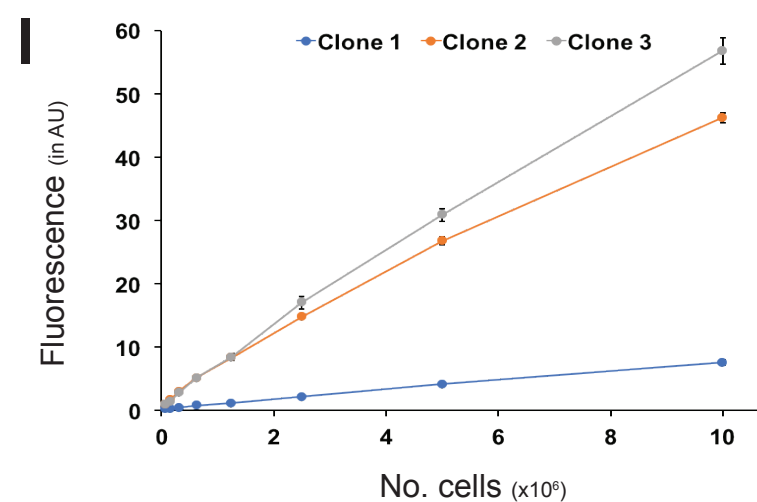
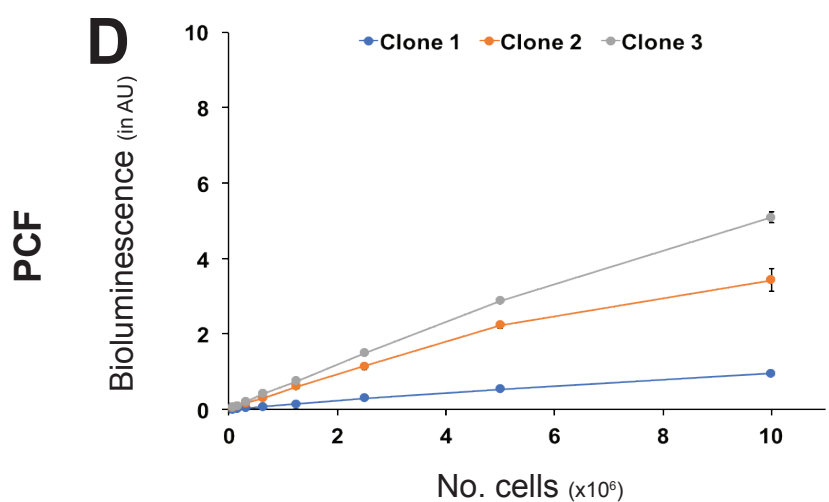
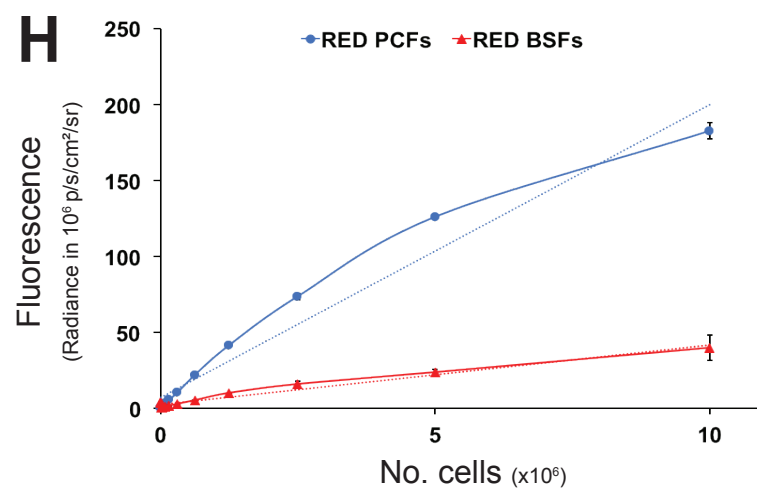
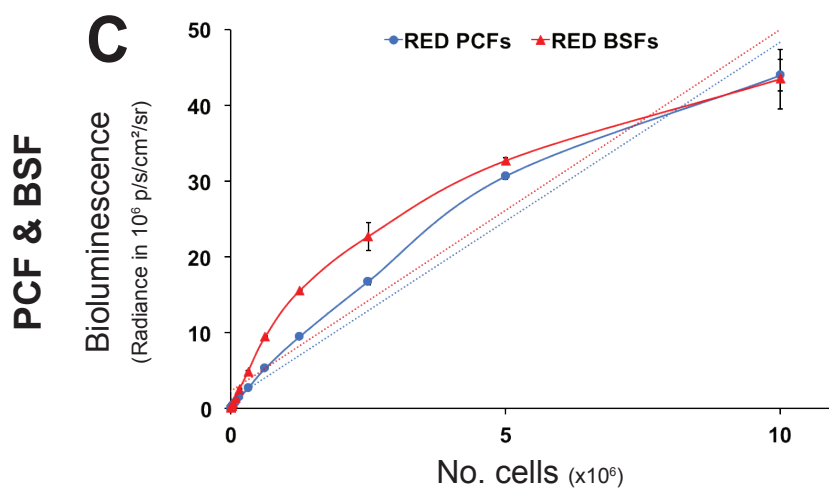
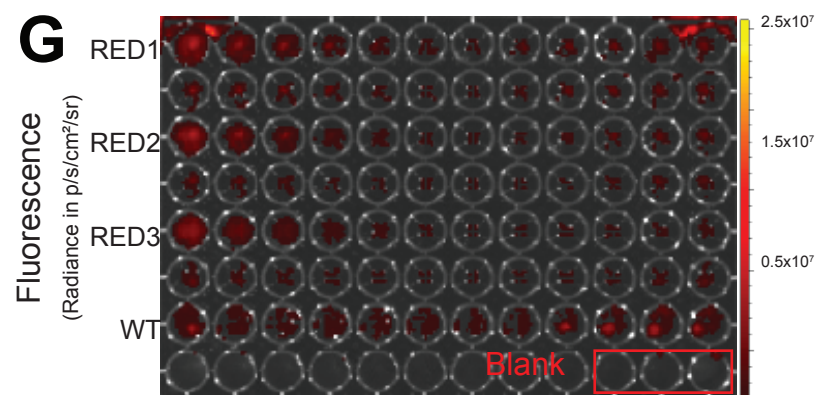
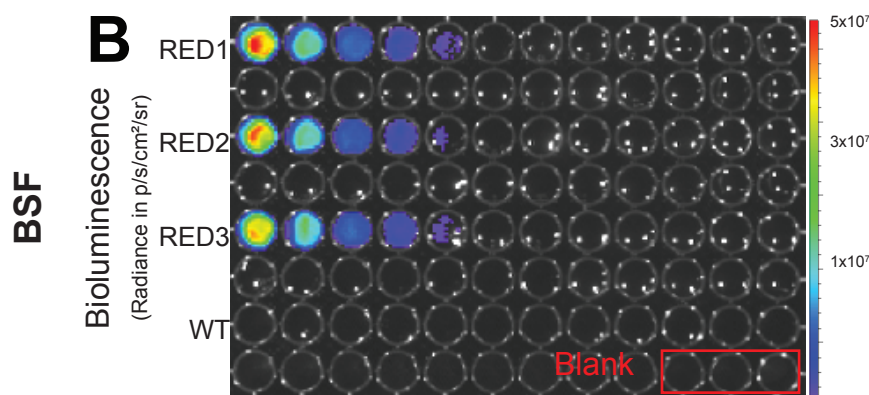
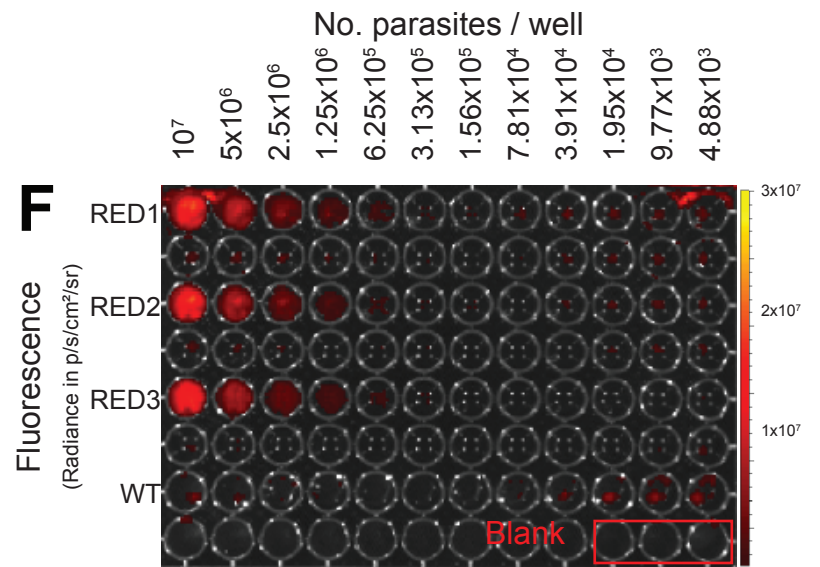
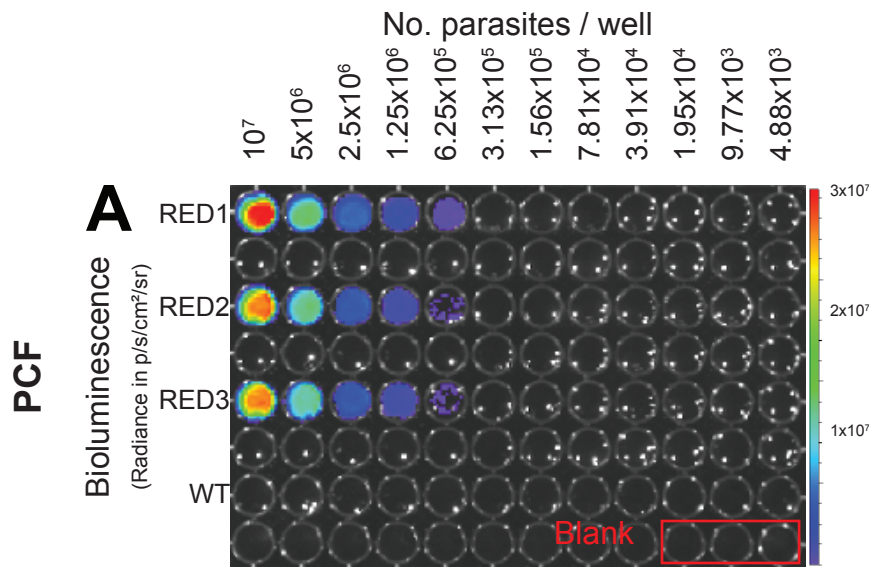
(Radiance in p/s/cm<sup>2</sup>/sr)

# Fluorescence

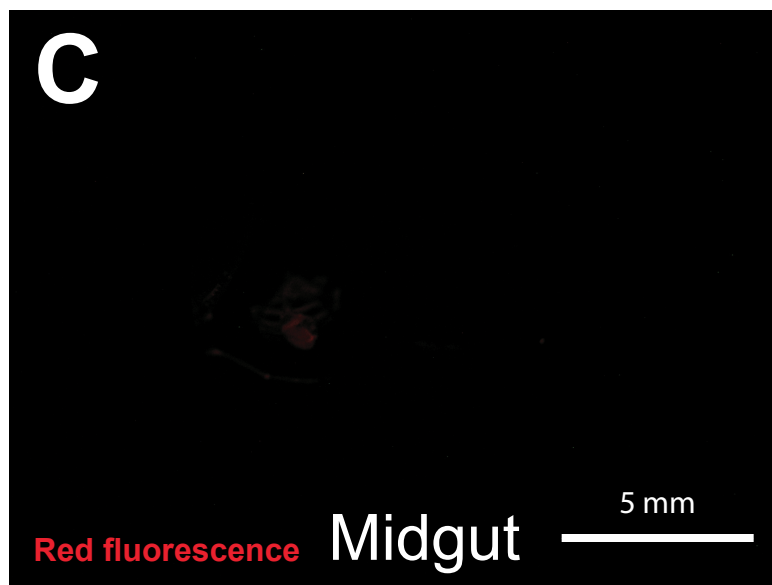
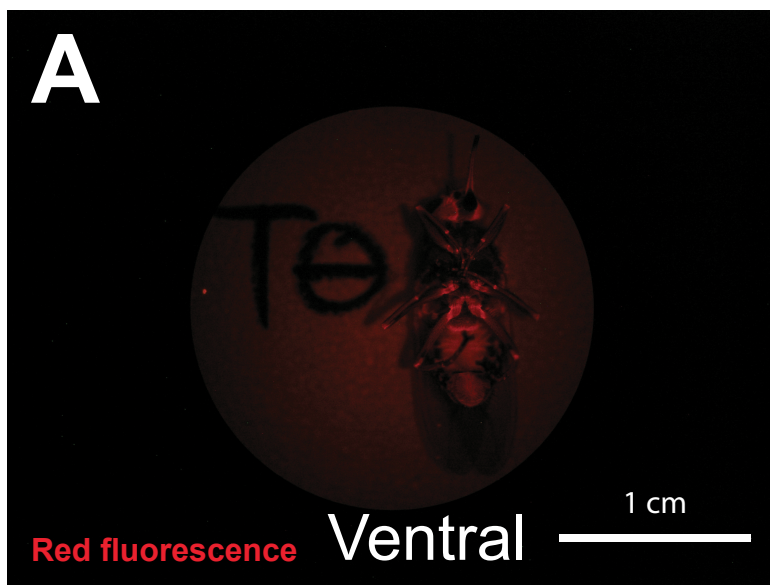
(Radiance in p/s/cm<sup>2</sup>/sr)

*In vivo imager*

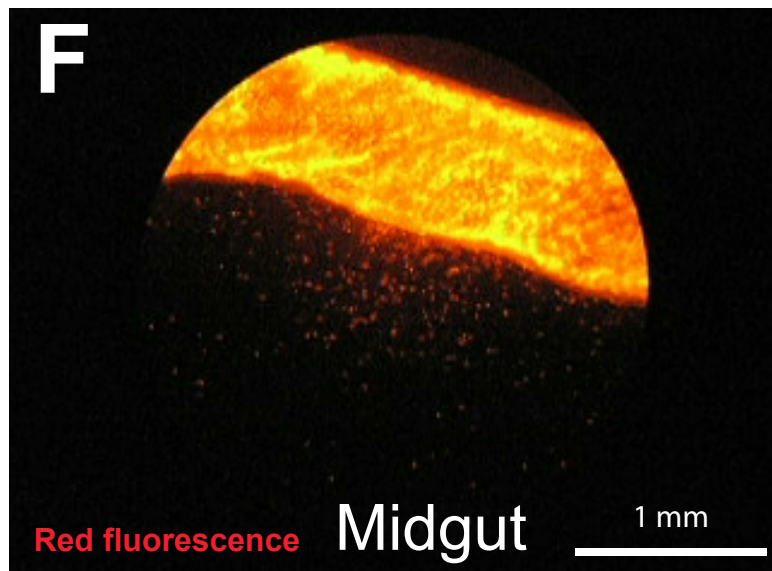
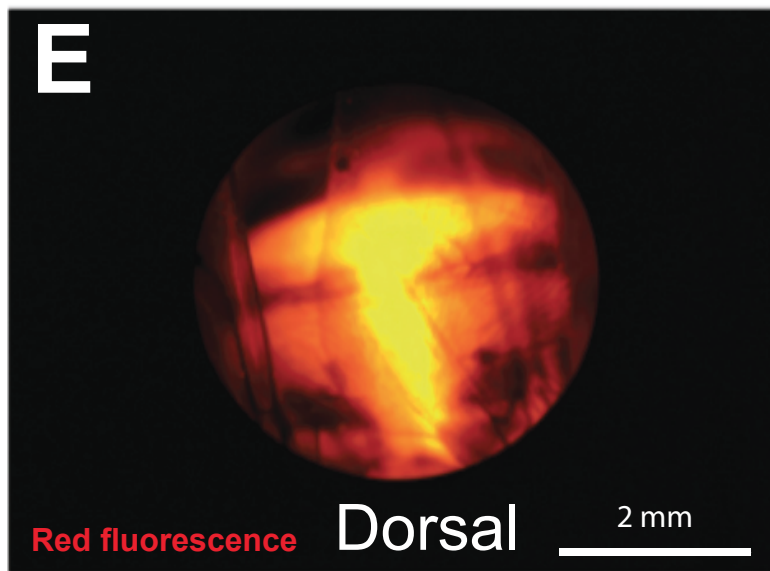
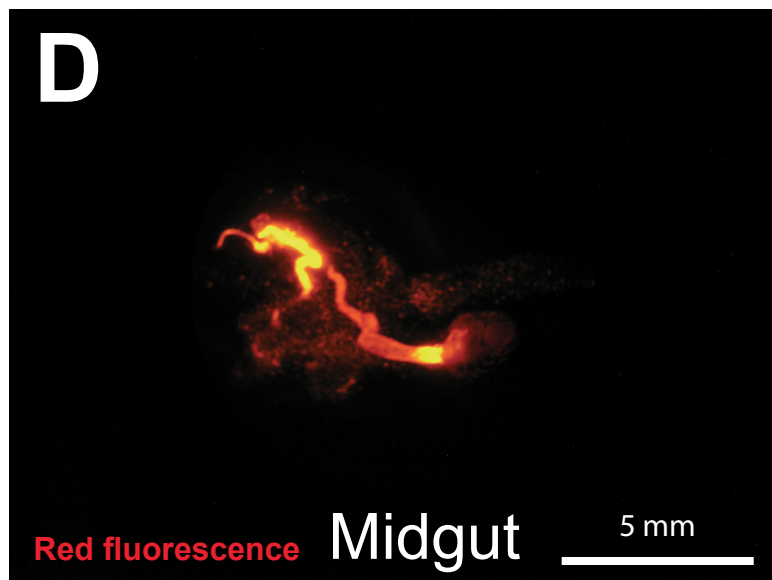
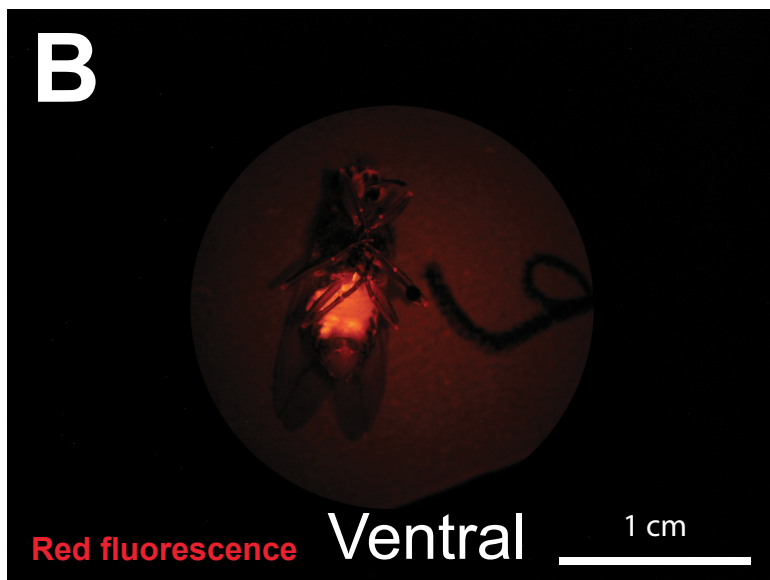
*In vitro plate reader*



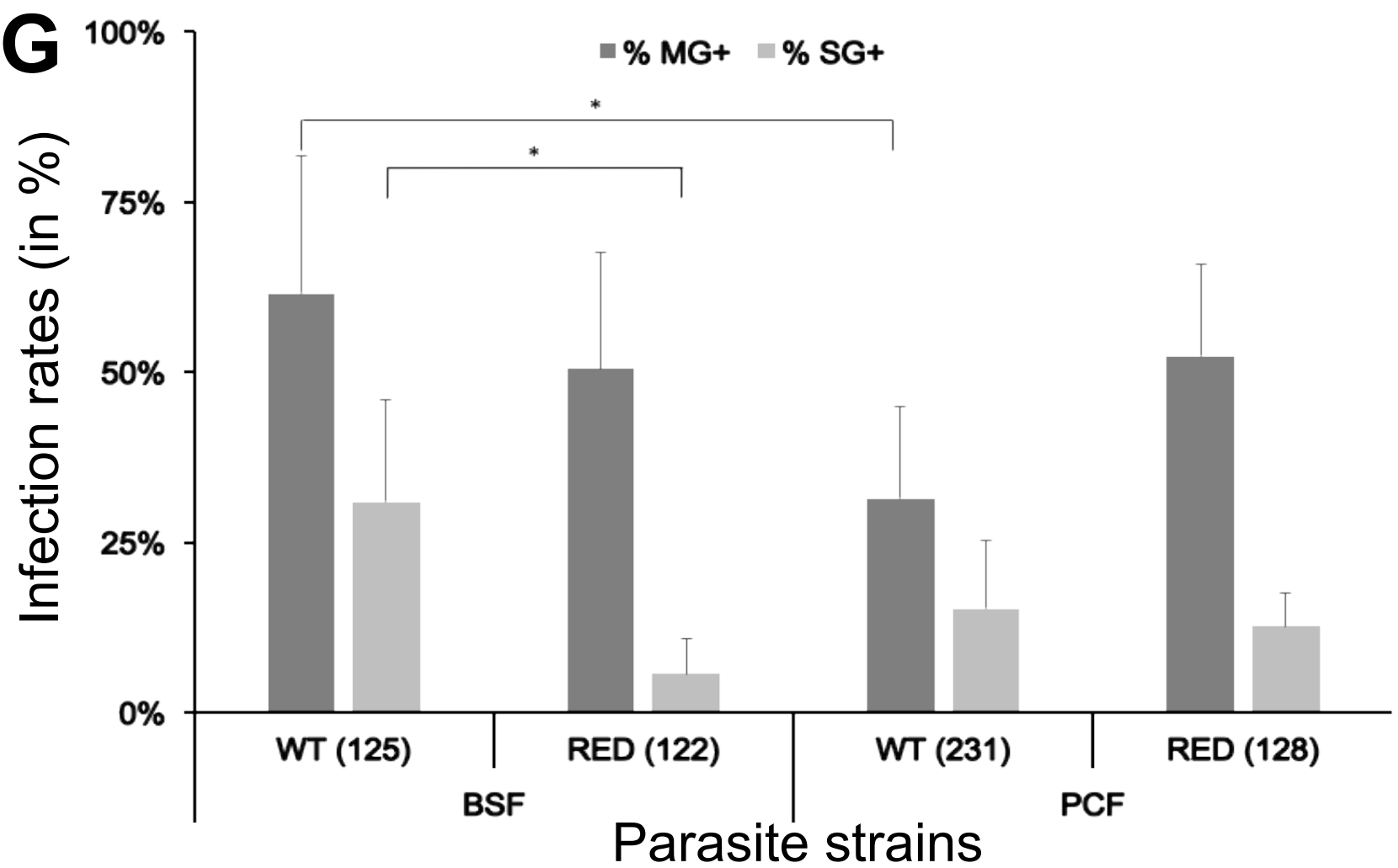
- RED parasites

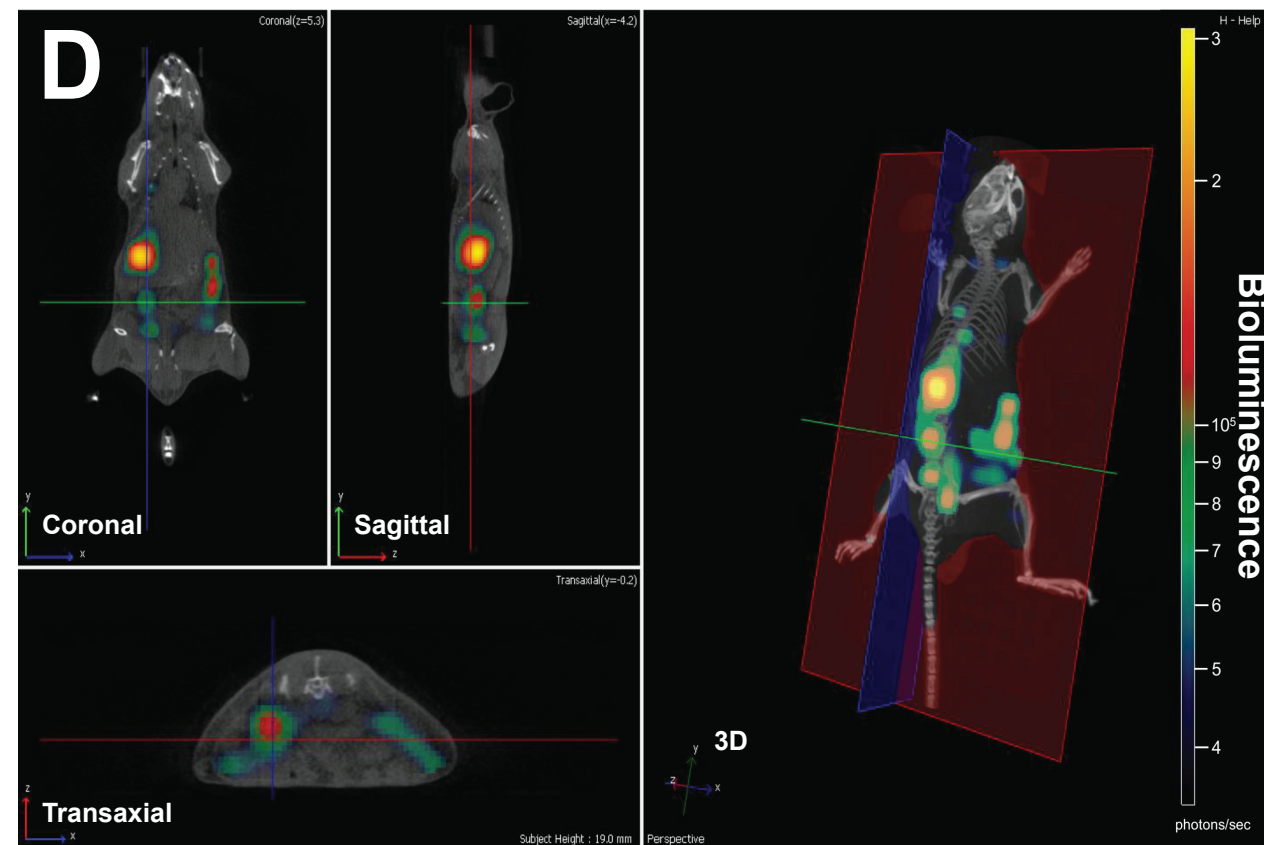
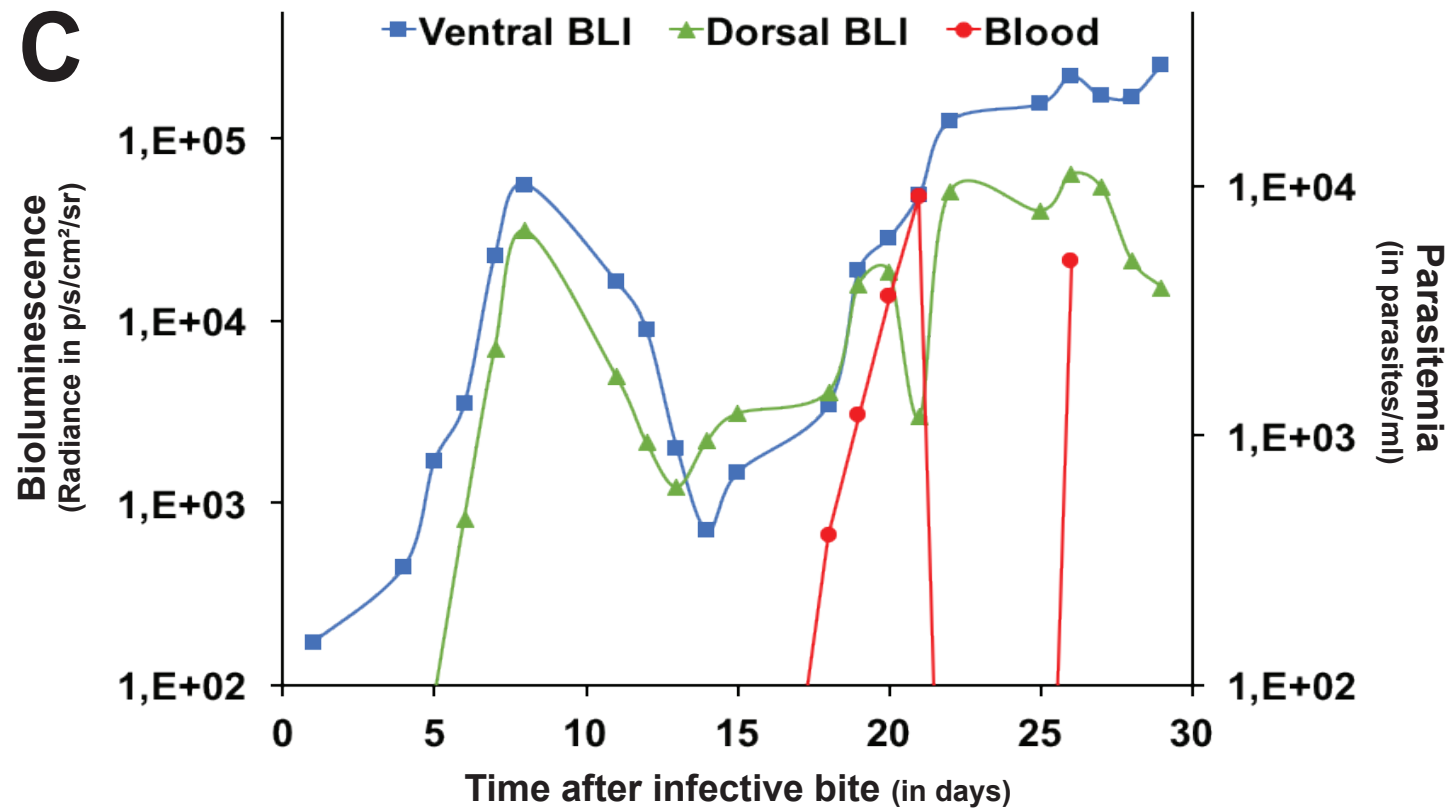
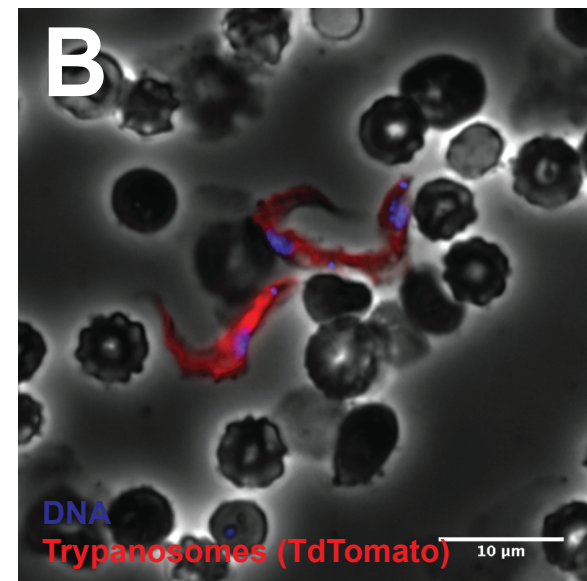
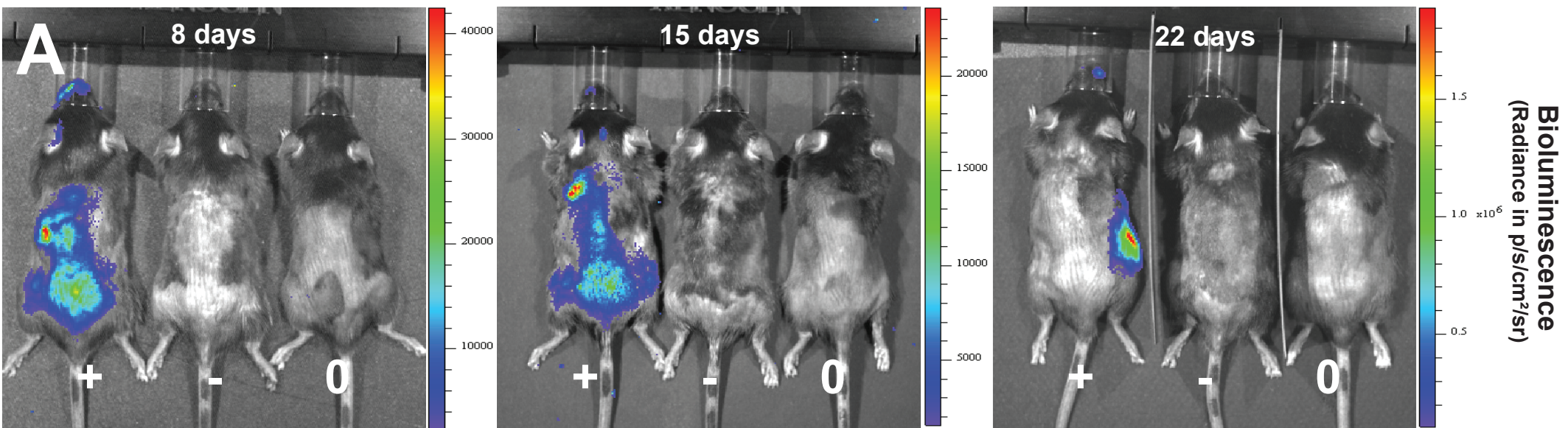


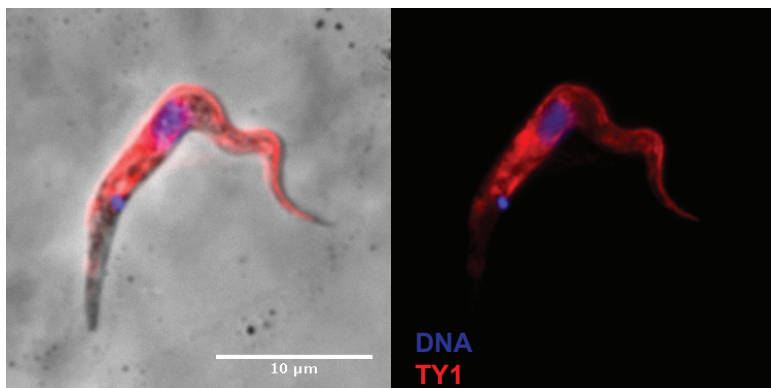
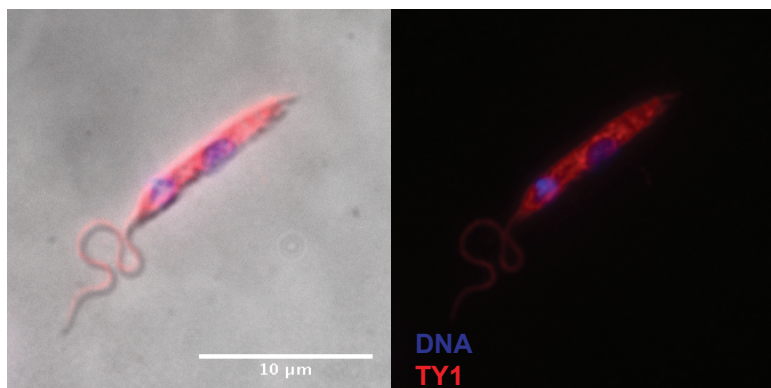
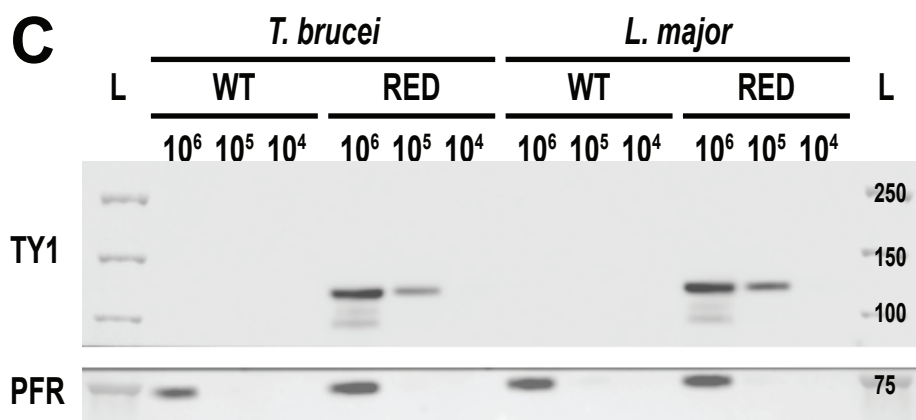
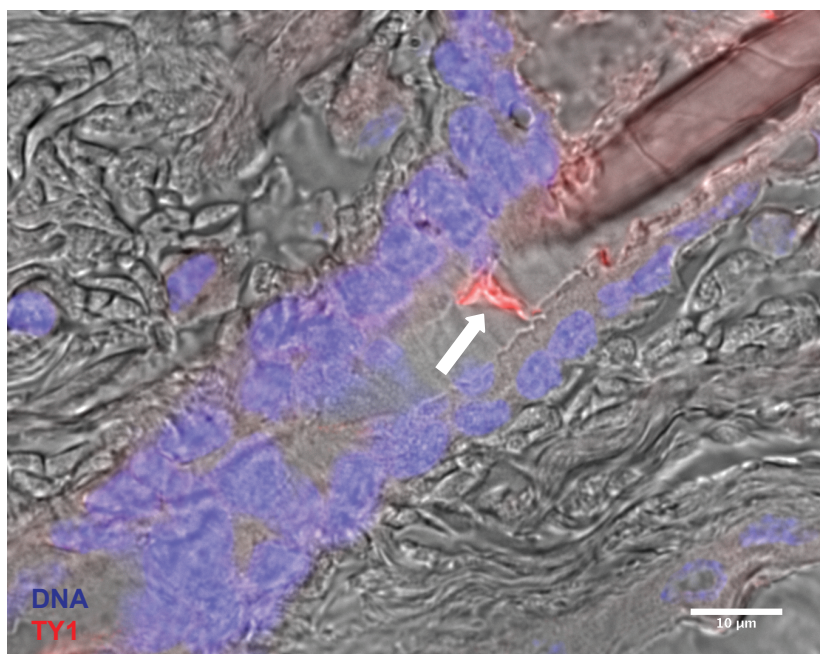
+ RED parasites



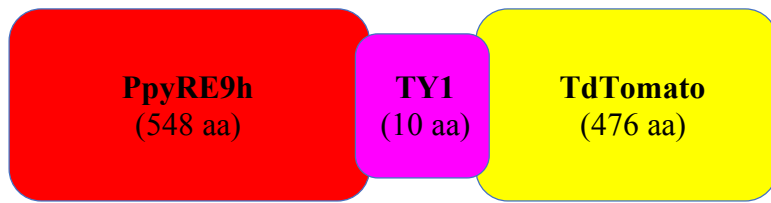
**G**





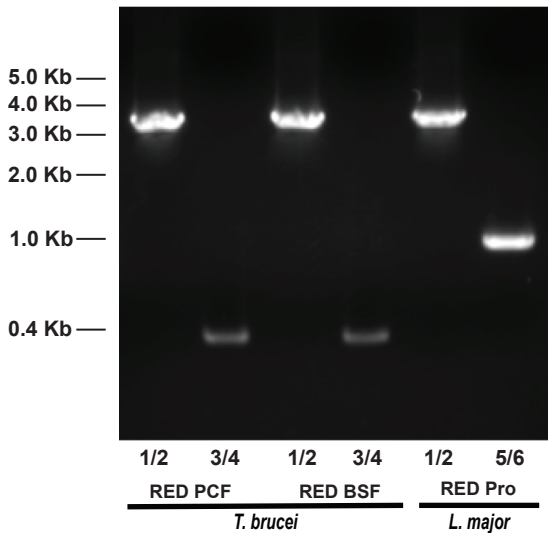
**A****B****C****D**

**A**



**B**

ATGGAGGACGCCAAGAACATCAAGAAGGGACCCAGCCCTTCTACCCCTGGAGGACGGCACAGCCGGCGAGCAGCTGCA  
CAAGGCCATGAAGCGGTACGCCCTGGTGCCAGGCACCATCGCCTTCACCGACGCCACATCGAGGTGAACATCACCTACG  
CCGAGTACTTCGAGATGAGCGTGCGGCTGGCCGAGGCCATGAAGCGGTACGGCCTGAACACCAACCACCGGATCGTGGTG  
TGCAGCGAGAACAGCCTGCAGTCTTTCATGCCCGTGCTGGGAGCCCTGTTTCATCGGCGTGGCCGTGGCCCGAGCCAACGA  
CATCTACAACGAGCGGGAGCTGCTGAACAGCATGAACATCAGCCAGCCACCCTGGTGTTCGTGAGCAAGAAGGGCCTGC  
AGAAGATCCTGAATGTGCAGAAGAAGCTGCCCATCATCCAGAAGATCATCATCATGGACAGCAAGACCGATTACCAGGGC  
TTCAGAGCATGTACACCTTCGTGACCAGCCACCTGCCCCAGGCTTCAACGAGTACGACTTCGTGCCCGAGAGCTTCGA  
CCGGGACAAGACCATCGCCCTGATCATGAACAGCAGCGGCAGCACCGGCCTGCCAAGGGCGTGGCCCTGCCCCACCGGG  
CCCTGTGCGTGCAGTTCAGCCACGCCAGAGACCCCATCTTCGGCAACCAGATCGCCCCGACACCGCCATCCTGAGCGTG  
GTGCCCTTCCACCAGGGCTTCGGCATGTTACCCACCCTGGGCTACCTGATCTGCGGCTTCGGGTGGTGTGATGTACAG  
GTTTCGAGGAGGAGCTGTTCTGCGGAGCCTGCAGGACTACAAGATCCAGACCGCCCTGCTGGTGCCACCCTGTTACAGT  
TCCTGGCCAAGAGCACCCCTGATCGACAAGTACGACCTGAGCAACCTGCACGAGATCGCCTCTGGCGGAGCCCCACTGAGC  
AAGGAGGTGGGCGAGGGCTGGCCAAGGGCTTCACCTGCCAGGCAATCCGGCAGGGCTACGGCCTGACCGAGACCACCAG  
CGCCATCCTGGTGACCCCATCGGCGACGACAAGCCCGGAGCCGTGGCAAGGTGGTCCCTTCTTCGAGGCCAAGGTGG  
TGGACCTGGACACCGGCAAGACCCTGGGCGTGAACCAGAGAGGGCGAGCTGTGCGTGAGAGGCCCATGATCATGAGCGGC  
TAGGTGAACAACCCCGAGGGCCACCAACGCCCTGATCGACAAGGACGGCTGGTGCACAGCGGGCAGATCGCCTACTGGGA  
CGAGGACGAGCACTTCTTCATCGTGGACCGGTGAAGAGCCTGATCAAGTACAAGGGCTACCAGGTGGCCCGAGCCGAGC  
TGGAGAGCATCCTGCTGCAGCACCCCAACATCCGGGACGCCGGAGTGGCCGACTGCCCGACGACGACGCGCGGAGAGCTG  
CCAGCCGCGTGGTGGTGTGCTGGAGCACGGCAAGACCATGACCGAGAAGGAGATCGTGGACTACGTGGCCAGCCAGGTGAC  
CACCGCCAAGAAGCTGAGAGGGCGGCTGGTGTTCGTGGACGAGGTGCCAAGGGCCTGACCGGCAAGCTGGACGCCAGAA  
AGATCCGGGAGATCCTGATCAAGGCCAAGAAGGGCGGCAAGATCGAGGTCCATACTAACCAGGACCCACTTGACaagctt  
ATGGTGAGCAAGGGCGAGGAGGTTCATCAAAGAGTTCATGCGCTTCAAGGTGCGCATGGAGGGCTCCATGAACGGCCACGA  
GTTTCGAGATCGAGGGCGAGGGCGAGGGCCGCCCTACGAGGGCACCCAGACCGCCAAGCTGAAGGTGACCAAGGGCGGCC  
CCCTGCCCTTCGCTGGGACATCCTGTCCCCCAGTTCATGTACGGCTCCAAGGCGTACGTGAAGCACCCCGCCGACATC  
CCCGATTACAAGAAGCTGTCTTCCCGAGGGCTTCAAGTGGGAGCGCGTGTGAACTTCGAGGACGGCGGTCTGGTGAC  
CGTGACCCAGGACTCCTCCCTGCAGGACGGCAGCGTGTACTACAAGGTGAAGATGCGCGGCACCAACTTCCCCCCGACG  
GCCCGTAATGCAGAAGAAGACCATGGGCTGGGAGGCTCCACCGAGCGCCTGTACCCCGCGACGGCGTGTGAAGGGC  
GAGATCCACCAGGCCCTGAAGCTGAAGGACGGCGGCCACTACCTGGTGGAGTTCAAGACCATCTACATGGCCAAGAAGCC  
CGTGCAACTGCCCGCTACTACTACGTGGACACCAAGCTGGACATCACCTCCCACAACGAGGACTACACCATCGTGGAAAC  
AGTACGAGCGCTCCGAGGGCCGCCACCACCTGTTCTGGGGCATGGCACCGGCAGCACCGGCAGCGGCAGCTCCGGCACC  
GCCTCCTCCGAGGACAACAACATGGCCGTATCAAAGAGTTCATGCGCTTCAAGGTGCGCATGGAGGGCTCCATGAACGG  
CCACGAGTTCGAGATCGAGGGCGAGGGCGAGGGCCGCCCTACGAGGGCACCCAGACCGCCAAGCTGAAGGTGACCAAGG  
GCGGCCCCCTGCCCTTCGCTGGGACATCCTGTCCCCCAGTTCATGTACGGCTCCAAGGCGTACGTGAAGCACCCCGCC  
GACATCCCCGATTACAAGAAGCTGTCTTCCCGAGGGCTTCAAGTGGGAGCGCGTGTGAACTTCGAGGACGGCGGTCT  
GGTGACCGTGAACCCAGGACTCCTCCCTGCAGGACGGCAGCTGATCTACAAGGTGAAGATGCGCGGCACCAACTTCCCCC  
CCGACGGCCCCGTAATGCAGAAGAAGACCATGGGCTGGGAGGCTCCACCGAGCGCCTGTACCCCGCGACGGCGTGTGCTG  
AAGGGCGAGATCCACCAGGCCCTGAAGCTGAAGGACGGCGGCCACTACCTGGTGGAGTTCAAGACCATCTACATGGCCAA  
GAAGCCCGTGAACCTGCCCGCTACTACTACGTGGACACCAAGCTGGACATCACCTCCCACAACGAGGACTACACCATCG  
TGGAACAGTACGAGCGCTCCGAGGGCCGCCACCACCTGTTCTGTACGGCATGGACGAGCTGTACAAGTAA

**A****B**